HAL open science

Bogoliubov Excitations Driven by Thermal Lattice Phonons in a Quantum Fluid of Light

Irénée Frérot, Amit Vashisht, Martina Morassi, Aristide Lemaître, Sylvain Ravets, Jacqueline Bloch, Anna Minguzzi, Maxime Richard

▶ **To cite this version:**

Irénée Frérot, Amit Vashisht, Martina Morassi, Aristide Lemaître, Sylvain Ravets, et al.. Bogoliubov Excitations Driven by Thermal Lattice Phonons in a Quantum Fluid of Light. Physical Review X, 2023, 13 (4), pp.041058. 10.1103/PhysRevX.13.041058 . hal-04381984v2

HAL Id: hal-04381984

https://hal.science/hal-04381984v2

Submitted on 10 Jan 2024

HAL is a multi-disciplinary open access archive for the deposit and dissemination of scientific research documents, whether they are published or not. The documents may come from teaching and research institutions in France or abroad, or from public or private research centers.

L'archive ouverte pluridisciplinaire **HAL**, est destinée au dépôt et à la diffusion de documents scientifiques de niveau recherche, publiés ou non, émanant des établissements d'enseignement et de recherche français ou étrangers, des laboratoires publics ou privés.

Bogoliubov Excitations Driven by Thermal Lattice Phonons in a Quantum Fluid of Light

Irénée Frérot,[1] Amit Vashisht,[2,3] Martina Morassi,[4] Aristide Lemaître,[4] Sylvain Ravets,[4] Jacqueline Bloch,[4] Anna Minguzzi,[2] and Maxime Richard[1,5,6,*]

[1]*University Grenoble Alpes, CNRS, Grenoble INP, Institut Néel, 38000 Grenoble, France*
[2]*University Grenoble Alpes, CNRS, LPMMC, 38000 Grenoble, France*
[3]*Center for Nonlinear Phenomena and Complex Systems, Université Libre de Bruxelles, CP 231, Campus Plaine, B-1050 Brussels, Belgium*
[4]*Centre de Nanosciences et de Nanotechnologies, CNRS, Université Paris-Sud, Université Paris-Saclay, 91120 Palaiseau, France*
[5]*Majulab International Research Laboratory, CNRS, National University of Singapore, Nanyang Technological University, Sorbonne Université, Université Côte d'Azur, 117543 Singapore*
[6]*Centre for Quantum technologies, National University of Singapore, 117543 Singapore*

(Received 2 May 2023; accepted 17 November 2023; published 26 December 2023)

The elementary excitations in weakly interacting quantum fluids have a nontrivial nature which is at the basis of defining quantum phenomena such as superfluidity. These excitations and the physics they lead to have been explored in closed quantum systems at thermal equilibrium both theoretically within the celebrated Bogoliubov framework and experimentally in quantum fluids of ultracold atoms. Over the past decade, the relevance of Bogoliubov excitations has become essential to understand quantum fluids of interacting photons. Their driven-dissipative character leads to distinct properties with respect to their equilibrium counterparts. For instance, the condensate coupling to the photonic vacuum environment leads to a nonzero generation rate of elementary excitations with many striking implications. In this work, considering that quantum fluids of light are often hosted in solid-state systems, we show within a joint theory-experiment analysis that the vibrations of the crystal constitute another environment that the condensate is fundamentally coupled to. This coupling leads to a unique heat transfer mechanism, resulting in a large generation rate of elementary excitations in typical experimental conditions, and to a fundamental nonzero contribution at vanishing temperatures. Our work provides a complete framework for solid-embedded quantum fluids of light, which is invaluable in view of achieving a regime dominated by photon-vacuum fluctuations.

DOI: 10.1103/PhysRevX.13.041058

Subject Areas: Condensed Matter Physics, Photonics, Quantum Physics

I. INTRODUCTION

Interactions between the constituent particles of a quantum fluid play a key role in their response to any space-time perturbations, such as thermal fluctuations, or an obstacle disrupting the quantum flow. They provide a many-body nature to the quantum fluid elementary excitations that results in spectacular macroscopic phenomena, such as superconductivity [1] and superfluidity [2,3]. While capturing in full generality many-body excitations represents a daunting theoretical challenge, the celebrated Bogoliubov theory provides a microscopic theoretical framework to describe them in bosonic quantum fluids in the weakly interacting regime, namely when the two-body scattering length is much shorter than the average interparticle distance. In this regime, the elementary excitations are transformed from free particles (operator $\hat{a}_{\mathbf{q}}$) to correlated particle-hole quasiparticles $\hat{\beta}_{\mathbf{q}} = u_{\mathbf{q}}\hat{a}_{\mathbf{q}} + v_{-\mathbf{q}}\hat{a}^{\dagger}_{-\mathbf{q}}$, where $(u_{\mathbf{q}}, v_{\mathbf{q}})$ are the characteristic Bogoliubov amplitudes and $\hbar\mathbf{q}$ is the excitation momentum [4,5].

This nontrivial nature and its consequences on a quantum fluid behavior is a strikingly rich research area that has been blossoming, in the context of closed quantum system at thermal equilibrium, for decades. In weakly interacting ultracold atoms, superfluidity [6], and the underlying linear dispersion relation of the elementary excitations [7], as well as the Bogoliubov transformation it stems from [8], were thus found experimentally in the early 2000s. Since then, the role of Bogoliubov excitations has been investigated and clarified in increasingly complex phenomena such as

*Corresponding author: maxime.richard@cnrs.fr

Published by the American Physical Society under the terms of the Creative Commons Attribution 4.0 International license. Further distribution of this work must maintain attribution to the author(s) and the published article's title, journal citation, and DOI.

decoherence [9], thermalization [10,11], and revival [12], or in quantum fluids lacking long-range order [13].

Over the past decade, the relevance of Bogoliubov excitations in the description of quantum fluids of light has become increasingly evident [14]. Their necessity emerges from the weakly interacting character of the photons within the fluid, from which a Bogoliubov theory can be rigorously derived [15]. This strong similarity with their closed equilibrium counterparts allows understanding the emergence of superfluidity in quantum fluids of light [16–18] as a result of the soundlike dispersion relation of the elementary excitation [15,19–21]. Interestingly, the driven-dissipative character of these quantum fluids also leads to a wealth of unique properties. For instance, unlike in closed systems, the system openness means that it is coupled to the external world, and in particular to the quantum fluctuations of the photonic vacuum. This coupling leads to a fundamental background generation rate of Bogoliubov excitations on top of the condensate, which is characterized by pairwise quantum correlations [22], with a wide range of applications in dynamical Casimir physics [23], in Hawking radiation simulators [24–28], or for the production of quantum states of light [22,29,30].

In this work, we highlight the fact that in many experimental realizations, the photon vacuum is not the only environment a quantum fluid of light is coupled to. Indeed, for practical purpose, quantum fluids of light are often formed within a solid-state environment such as a nonlinear optical resonators [19,31], or a polaritonic semiconductor microcavity [14,32], such that the effective two-body interaction is conveniently provided by dressing the photons with a material electronic transition. In the latter case, photons and bound electron-hole pairs (excitons) are fully hybridized into exciton polaritons (hereafter simply referred to as polaritons), as considered in this work. In the present work, we study both theoretically and experimentally the steady-state flux of Bogoliubov excitations generated on top of a polariton condensate as a result of its coupling to photon vacuum, and to thermal lattice phonons (Fig. 1). We show that the solid-state environment, which at first sight could seem anecdotic for photonlike particles, has in fact a profound influence on the condensate properties. Indeed, the crystal lattice vibrations constitute a second full-fledged environment that the condensate is coupled to, and that provides its own contribution of fundamental background excitations on top of the condensate. We show that in our experimental conditions, this contribution not only dominates over the one of the photon-vacuum fluctuations, but that it also offers a unique opportunity to probe the particle-hole nature of the Bogoliubov excitations themselves. In addition, we evidence that the corresponding nonequilibrium thermal energy flowing between the thermal lattice phonons and the condensate is significantly attenuated by the Bogoliubov transformation. By theoretical extension of our model to $T = 0$ K, we demonstrate that the most fundamental state of the condensate always involves a contribution of the lattice

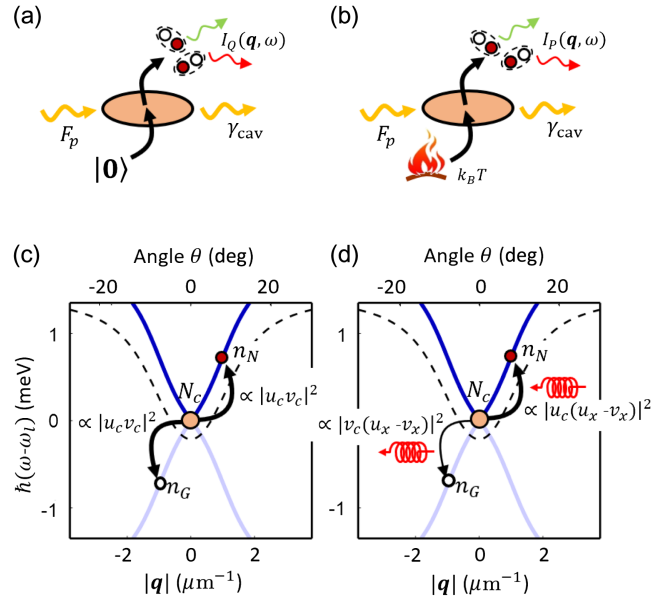

FIG. 1. Sketch of the two intrinsic mechanisms creating Bogoliubov excitations in a quantum fluid of light embedded in a finite-temperature solid-state microresonator. Panel (a) describes the contribution resulting from the coupling to the extra cavity photon vacuum (noted $|0\rangle$ in the sketch). Panel (b) describes the contribution resulting from the coupling to the bath of lattice phonons at temperature T (symbolized as a fire). The experimental configuration considered in this work consists in a steady-state condensate (orange ellipse) involving $\langle N_c\rangle$ photonlike particles (exciton polaritons) pumped at resonance by a laser field of amplitude F_p, and subject to a loss rate $\gamma_{\rm cav}$. The correlated particle-hole nature of Bogoliubov excitations is shown as bound red and white symbols. The radiative recombination of the latter is shown as escaping photons. The photons' spectral functions $I_{Q,P}(\mathbf{q},\omega)$ are derived in Sec. II and given in Eqs. (22) and (25), respectively. Panels (c) and (d) describe the same mechanism as (a) and (b), using the dispersion relations in the framework of Bogoliubov theory, which consists of a normal (dark blue) and ghost (light blue) mode, both with a shape that differs from the free polaritons dispersion relation (dashed line). As discussed in the main text, the spontaneous emission rate of Bogoliubov excitations is proportional to $|u_c v_c|^2$ when they result from coupling to the photon-vacuum fluctuations (c), and to $|u_c(u_x - v_x)|^2$ $[|v_c(u_x - v_x)|^2]$ for the normal [ghost] mode, when they result from coupling to thermal lattice phonons (d), where $(u_{c,x}, v_{c,x})$ are the coefficients of the Bogoliubov transformation. The subscript c (x) refers to the cavity photon (exciton) component of a Bogoliubov excitation.

phonon vacuum, alongside the photon-vacuum contribution. Finally, we determine a crossover temperature below which the generation of elementary excitations is dominated by the photonic vacuum, which is a necessary condition for the generation of quantum correlations within the condensate excitation spectrum.

We organize this article as follows. In Sec. II, we develop a Bogoliubov theory of a resonantly driven exciton-polariton condensate, coupled both to lattice phonons and to free

space photons. The observables relevant to the experiment are calculated, such as the spectral function of the elementary excitation emission $I(\mathbf{q},\omega)$. We report in Sec. III our measurement of $I(\mathbf{q},\omega)$ in a microcavity between temperatures of 6.6 and 12 K. By quantitative comparison with the theory, we extract the elementary excitation dispersion relation (Sec. II C) and the Bogoliubov transformation amplitudes $(u_{\mathbf{q}}, v_{-\mathbf{q}})$ (Sec. III D). In the discussion Sec. IV, we estimate the experimentally achieved Bogoliubov-transformation-induced decoupling from the phonon bath and derive a crossover temperature below which the photon-vacuum fluctuations are expected to overcome the lattice phonons fluctuations. We discuss how to tune the microcavity parameters to achieve a refined control over both phenomena. Finally, Sec. V offers some concluding remarks.

II. THEORY

A. Microscopic model and observables

In this work, we investigate a quantum fluid of light consisting of resonantly driven exciton polaritons [14,32] (henceforth denoted as "polaritons"), namely, hybrid quasiparticles obtained when photons confined in a cavity are in the strong coupling regime with an excitonic transition (bound electron-hole pairs) provided by a semiconductor planar quantum well. Their excitonic component provides them with two-body interactions, as well as interactions with the bath of acoustic solid-state lattice phonons, while the photonic fraction mediates the coupling to the resonant laser drive and to the extracavity free propagating photons that constitute the measured observable. The Hamiltonian describing all these interactions expressed in the exciton-photon basis thus consists of the following contributions:

$$\hat{\mathcal{H}} = \hat{\mathcal{H}}^{(0)}_{\mathrm{pol}} + \hat{\mathcal{V}}_{xx} + \hat{\mathcal{V}}_{\mathrm{sat}} + \hat{\mathcal{H}}^{(0)}_{\mathrm{ph}} + \hat{\mathcal{V}}_{xp} + \hat{\mathcal{V}}_{\mathrm{out}}, \quad (1)$$

where

$$\hat{\mathcal{H}}^{(0)}_{\mathrm{pol}} = \hbar\sum_{\mathbf{q}}\left[\omega_{x,\mathbf{q}}\hat{b}^{\dagger}_{\mathbf{q}}\hat{b}_{\mathbf{q}} + \omega_{c,\mathbf{q}}\hat{a}^{\dagger}_{\mathbf{q}}\hat{a}_{\mathbf{q}} + \frac{\Omega}{2}(\hat{a}^{\dagger}_{\mathbf{q}}\hat{b}_{\mathbf{q}} + \mathrm{H.c.})\right] + [f_p(t)^*\hat{a}_{\mathbf{q}_p} + \mathrm{H.c.}] \quad (2)$$

describes the interaction between cavity photons (operator $\hat{a}_{\mathbf{q}}$) and quantum well excitons ($\hat{b}_{\mathbf{q}}$) of in-plane momentum $\mathbf{q}$, in which the strong coupling regime is described by the third term in the sum, with $\hbar\Omega$ being the Rabi splitting [33,34] separating the upper and lower polariton modes when $\hat{\mathcal{H}}^{(0)}_{\mathrm{pol}}$ is in its diagonal form [35]. The last term in $\hat{\mathcal{H}}^{(0)}_{\mathrm{pol}}$ describes the coherent laser drive with $f_p(t) = F_p e^{i\omega_{\mathrm{las}}t}$ of amplitude F_p with corresponding in-plane momentum $\hbar\mathbf{q}_p$. Concerning the interaction terms, we take

$$\hat{\mathcal{V}}_{xx} = (\hbar g_x/2)\sum_{\mathbf{k},\mathbf{k}',\mathbf{q}}\hat{b}^{\dagger}_{\mathbf{k}+\mathbf{q}}\hat{b}^{\dagger}_{\mathbf{k}'-\mathbf{q}}\hat{b}_{\mathbf{k}'}\hat{b}_{\mathbf{k}}. \quad (3)$$

This describes the Coulomb-mediated interaction between excitons, of strength g_x, that contributes to two-body interactions between polaritons [36]. Furthermore,

$$\hat{\mathcal{V}}_{\mathrm{sat}} = (-\hbar g_s/2)\sum_{\mathbf{k},\mathbf{k}',\mathbf{q}}(\hat{a}^{\dagger}_{\mathbf{k}+\mathbf{q}}\hat{b}^{\dagger}_{\mathbf{k}'-\mathbf{q}}\hat{b}_{\mathbf{k}'}\hat{b}_{\mathbf{k}} + \mathrm{H.c.}) \quad (4)$$

describes an additional interaction mechanism between excitons of strength g_s and often referred to as saturation nonlinearity. It results from the fact that excitons consist of bound fermions, namely electrons and holes, so that the creation of an exciton produces a nonzero fermionic phase-space filling, that in turn reduces the photon-creation probability of a second exciton [37]. The term

$$\hat{\mathcal{H}}^{(0)}_{\mathrm{ph}} = \hbar\sum_{\mathbf{q},k_z}\omega^{(\mathrm{ph})}_{\mathbf{q},k_z}\hat{c}^{\dagger}_{\mathbf{q},k_z}\hat{c}_{\mathbf{q},k_z} \quad (5)$$

describes the three-dimensional continuum of harmonic longitudinal lattice vibration modes or longitudinal acoustic (LA) phonons, with bosonic operators $\hat{c}_{\mathbf{q},k_z}$. $\omega^{(\mathrm{ph})}_{\mathbf{q},k_z} = v_s\sqrt{\mathbf{q}^2 + k_z^2}$ is the phonon dispersion relation, with v_s the LA phonons' sound velocity. Transverse acoustic phonons have a much weaker coupling strength with excitons [38] and are thus neglected thereafter. $\mathbf{q} = (q_x, q_y)$ is the two-dimensional momentum in the plane of the microcavity spacer and quantum well, and k_z is in the orthogonal direction. The interaction between excitons and LA phonons is dominated by the elastic deformation potential and reads [39,40]:

$$\hat{\mathcal{V}}_{xp} = i\hbar\sum_{\mathbf{q},k_z}g_{xp}(\mathbf{q},k_z)(\hat{c}_{\mathbf{q},k_z} - \hat{c}^{\dagger}_{-\mathbf{q},k_z})\sum_{\mathbf{q}'}\hat{b}^{\dagger}_{\mathbf{q}+\mathbf{q}'}\hat{b}_{\mathbf{q}'}, \quad (6)$$

where $g_{xp}(\mathbf{q},k_z)$ is the momentum-dependent interaction strength. The detailed expression for $g_{xp}(\mathbf{q},k_z)$ is given in Appendix A 9. Finally, the term

$$\hat{\mathcal{V}}_{\mathrm{out}} = \hbar\sum_{\mathbf{q},k_z}\{\omega^{(\alpha)}_{\mathbf{q},k_z}\hat{\alpha}^{\dagger}_{\mathbf{q},k_z}\hat{\alpha}_{\mathbf{q},k_z} + \kappa[\hat{\alpha}^{\dagger}_{\mathbf{q},k_z}\hat{a}_{\mathbf{q}} + \mathrm{H.c.}]\} \quad (7)$$

describes the conversion of intracavity photons into extracavity free propagating photons, described by the bosonic operator $\hat{\alpha}_{\mathbf{q},k_z}$. Cavity photons can tunnel at a rate κ into this continuum across the mirrors, and vice versa, as a result of the finite reflectivity of the mirrors. κ is safely considered constant within the momentum and frequency range of the experiment. The first term in Eq. (7) describes the extracavity free propagating photon energy, whose dispersion relation in vacuum is $\omega^{(\alpha)}_{\mathbf{q},k_z} = c\sqrt{\mathbf{q}^2 + k_z^2}$ with c the speed of light. The second term describes the tunnel coupling mechanism.

The experimental observable of focus in the current work is the extracavity photon intensity $I(\mathbf{q},\omega)$ resolved both in

frequency and momentum. Using an input-output formalism detailed in Appendix A 1 we derive a general relation between the intracavity photon field and the extracavity photon intensity that simplifies into

$$I(\mathbf{q},\omega) = \frac{\gamma_{\rm cav}}{\pi}\int_{-\infty}^{+\infty} d\tau e^{-i\omega\tau}\langle \hat{a}^\dagger_{\mathbf{q}}(\tau)\hat{a}_{\mathbf{q}}(0)\rangle, \tag{8}$$

where we have used the fact that the extracavity photons are in a vacuum state (an excellent approximation considering that our photons are in the ~1.5 eV energy range), and considered that the system has reached a steady state as is the case in the experiment. $\gamma_{\rm cav} \propto \kappa^2$ is the cavity loss rate (see Appendix A 1 for further details). We thus proceed to derive the two-time correlator $\langle \hat{a}^\dagger_{\mathbf{q}}(\tau)\hat{a}_{\mathbf{q}}(0)\rangle$ in the presence of both photon-vacuum fluctuations and a thermal population of acoustic phonons.

In our experimental configuration, polariton-polariton interactions are relatively weak, i.e., the associated scattering length is much smaller than the interparticle distance, and the driving laser intensity is large enough to induce a macroscopic population of the steady-state excitonic and photonic modes [5]. This justifies a mean-field treatment for the condensate and the Bogoliubov approximation for the description of the excitations on top of it.

B. Bogoliubov theory

1. Mean-field equation for the condensate

We first need to determine the mean-field steady state of the system. Writing the Heisenberg equations of motion for the cavity photons and excitons at the laser wave vector $\mathbf{q}_p$, and setting, as per the mean-field approximation, $\langle \hat{b}_{\mathbf{q}_p}\rangle = \psi_x$ and $\langle \hat{a}_{\mathbf{q}_p}\rangle = \psi_c$, we find the steady-state equations:

$$\begin{aligned}&(\omega_x - i\gamma_x/2 + g_x|\psi_x|^2)\psi_x \\ &\quad + (\Omega/2 - g_s|\psi_x|^2)\psi_c - g_s\psi_x^2\psi_c^* = 0\end{aligned} \tag{9}$$

and

$$(\omega_c - i\gamma_{\rm cav}/2)\psi_c + (\Omega/2 - g_s|\psi_x|^2/2)\psi_x + F_p = 0, \tag{10}$$

where $n_{x,c} = |\psi_{x,c}|^2$ are the excitonic and photonic densities and from here on the excitonic and photonic frequencies are shifted by the laser frequency $\omega_{\rm las}$. For details on the full solution to Eqs. (9) and (10), see Appendix A 2.

Note that we have introduced a phenomenological decoherence rate for the excitonic transition of the form $\gamma_x(\mathbf{q}) = \gamma_{x,0} + \beta q^2$ $(\beta > 0)$ that describes in an effective way the fact that polaritons of higher energy (and hence of higher $|\mathbf{q}|$) interact more strongly with the quantum well imperfections (see, e.g., Refs. [41–43] for details). We do not attempt to describe this effect in our model as it would far exceed our scope without clear benefit for the purpose of this work.

2. Bogoliubov approximation

We then use the Bogoliubov approximation to reduce the interaction terms to a quadratic form. This approximation amounts to (i) assume that both the cavity photon and the exciton modes at the laser momentum $\mathbf{q}_p$ are macroscopically occupied and (ii) neglect in the Hamiltonian terms involving more than two operators at $\mathbf{q} \neq \mathbf{q}_p$. We thus derive the resulting quadratic exciton-exciton interaction terms $\hat{\mathcal{V}}_{xx}$ and $\hat{\mathcal{V}}_{\rm sat}$ that describe interactions occurring within the condensate, and with final states outside the condensate with momenta $\mathbf{q}_p + \mathbf{q}$ and $\mathbf{q}_p - \mathbf{q}$ (see Appendix A 3 for the detailed expression). The phonon-exciton interaction becomes

$$\hat{\mathcal{V}}_{xp} = i\hbar\sqrt{n_x}\sum_{\mathbf{q},k_z} g_{xp}(\mathbf{q},k_z)(\hat{c}_{\mathbf{q},k_z} - \hat{c}^\dagger_{-\mathbf{q},k_z})(\hat{b}^\dagger_{\mathbf{q}_p+\mathbf{q}} + \hat{b}_{\mathbf{q}_p-\mathbf{q}}) \tag{11}$$

and describes the scattering of a condensate exciton via emission or absorption of a phonon into an excited state with momentum $\mathbf{q}_p + \mathbf{q}$ or $\mathbf{q}_p + \mathbf{q}$. This term represents a key ingredient in this work, as it describes the condensate interaction with the solid-state environment.

Under the Markov approximation for the damping kernel associated to the bath of extracavity photons and the bath of solid-state phonons, the excitations take the following final form (see Appendixes A 4–A 7 for details):

$$\hat{\mathcal{A}}_{\mathbf{q}_p,\mathbf{q}}(\omega) = i[\omega\mathbf{1} - M_{\mathbf{q}}]^{-1}\hat{\mathcal{F}}_{\mathbf{q}_p,\mathbf{q}}, \tag{12}$$

where we have set for shorthand notation,

$$\hat{\mathcal{A}}_{\mathbf{q}_p,\mathbf{q}}(\omega) = [\hat{a}_{\mathbf{q}_p+\mathbf{q}}(\omega), \hat{b}_{\mathbf{q}_p+\mathbf{q}}(\omega), \hat{a}^\dagger_{\mathbf{q}_p-\mathbf{q}}(\omega), \hat{b}^\dagger_{\mathbf{q}_p-\mathbf{q}}(\omega)]^T, \tag{13}$$

and introduced the Langevin force vector:

$$\begin{aligned}\hat{\mathcal{F}}_{\mathbf{q}_p,\mathbf{q}}(\omega) = [&\hat{F}_{\mathbf{q}_p+\mathbf{q}}(\omega), \hat{f}_{\mathbf{q}}(\omega) - \hat{f}^\dagger_{-\mathbf{q}}(\omega), \\ &\hat{F}^\dagger_{\mathbf{q}_p-\mathbf{q}}(\omega), f^\dagger_{-\mathbf{q}}(\omega) - \hat{f}_{\mathbf{q}}(\omega)]^T.\end{aligned} \tag{14}$$

The matrix $M_{\mathbf{q}}$ reads:

$$M_{\mathbf{q}} = \begin{pmatrix} \omega_{c,\mathbf{q}_p+\mathbf{q}} - i\gamma_{\mathrm{cav}} & -2\mu_s + \Omega/2 & 0 & -\mu_s \\ -2\mu_s + \Omega/2 & \omega_{x,\mathbf{q}_p+\mathbf{q}} - i\gamma_{x,\mathbf{q}_p+\mathbf{q}} + 2\mathrm{Re}(\mu_{sx}) & -\mu_s & \mu_{sx} \\ 0 & \mu_s & -\omega_{c,\mathbf{q}_p-\mathbf{q}} - i\gamma_{\mathrm{cav}} & 2\mu_s - \Omega/2 \\ \mu_s & -\mu_{sx}^* & 2\mu_s - \Omega/2 & -\omega_{x,\mathbf{q}_p-\mathbf{q}} - i\gamma_{x,\mathbf{q}_p-\mathbf{q}} - 2\mathrm{Re}(\mu_{sx}) \end{pmatrix}, \tag{15}$$

with $\mu_s = g_s n_x/2$ and $\mu_{sx} = g_x n_x - g_s\sqrt{n_x n_c}e^{-i\phi}$.

The Langevin force for cavity photons, that results from their coupling to the extracavity photons, reads:

$$\hat{F}_{\mathbf{q}}(t) = -i\sum_{k_z}\kappa_{\mathbf{q},k_z}\hat{\alpha}^{(\mathrm{in})}_{\mathbf{q},k_z}e^{-i\omega^{(\alpha)}_{\mathbf{q},k_z}t}, \tag{16}$$

where $\hat{\alpha}^{(\mathrm{in})}_{\mathbf{q},k_z} := e^{i\omega^{(\alpha)}_{\mathbf{q},k_z}t_0}\hat{\alpha}_{\mathbf{q},k_z}(t_0)$, with $t_0 \to -\infty$ a reference initial time. As discussed below, this force stems from the photon-vacuum fluctuations. Similarly, the Langevin force acting on excitons, as a result of their coupling to the thermal phonons bath, is

$$\hat{f}_{\mathbf{q}}(t) = \sqrt{n_x}\sum_{k_z}g_{xp}(\mathbf{q},k_z)\hat{c}^{(\mathrm{in})}_{\mathbf{q},k_z}e^{-i\omega^{(\mathrm{ph})}_{\mathbf{q},k_z}t}, \tag{17}$$

where $\hat{c}^{(\mathrm{in})}_{\mathbf{q},k_z} := \hat{c}_{\mathbf{q},k_z}(t_0)e^{i\omega^{(\mathrm{ph})}_{\mathbf{q},k_z}t_0}$. Similar equations of motion have been derived in the literature [29,44], but to the best of our knowledge, so far the interaction with lattice phonons has not been included.

3. Bogoliubov eigenmodes

Equations (12)–(15) describe how the cavity photons and excitons hybridize due to (i) the exciton-photon Rabi coupling Ω and (ii) two-body interactions, as well as their forcing by coupling to lattice phonons, decoherence via the excitonic component, and dissipation into extracavity photons. The $M_{\mathbf{q}}$ matrix is readily brought onto a diagonal form by $P_{\mathbf{q}}M_{\mathbf{q}}P_{\mathbf{q}}^{-1}$. The $P_{\mathbf{q}}$ matrix, whose explicit definition is given in Appendix A 7, contains the u, v coefficients of the Bogoliubov transformation. In particular, the (bosonic) lower polariton operator reads:

$$\hat{\beta}_{\mathrm{LP}c,\mathbf{q}_p+\mathbf{q}} = u_{\mathrm{LP},c,\mathbf{q}_p+\mathbf{q}}\hat{a}_{\mathbf{q}_p+\mathbf{q}} + u_{\mathrm{LP},x,\mathbf{q}_p+\mathbf{q}}\hat{b}_{\mathbf{q}_p+\mathbf{q}} + v_{\mathrm{LP},c,\mathbf{q}_p-\mathbf{q}}\hat{a}^\dagger_{\mathbf{q}_p-\mathbf{q}} + v_{\mathrm{LP},x,\mathbf{q}_p-\mathbf{q}}\hat{b}^\dagger_{\mathbf{q}_p-\mathbf{q}}. \tag{18}$$

There are thus four Bogoliubov coefficients per mode in our model instead of the usual two in the Bogoliubov theory. This is because the bosonic quasiparticles that constitute our condensate are exciton-photon hybrids, such that $u_{j,x}$, for instance, characterizes both the particle and the excitonic contribution of the Bogoliubov state in mode j, $v_{j,c}$ the hole and photonic contributions, and so on. In order to ensure bosonic commutation relations of the new quasiparticle field operators, the Bogoliubov coefficients are normalized according to $|u_{c,\mathbf{q}}|^2 + |u_{x,\mathbf{q}}|^2 - |v_{c,-\mathbf{q}}|^2 - |v_{x,-\mathbf{q}}|^2 = 1$ for all modes. For the sake of compactness, we drop the $\mathbf{q}_p$ dependence as well as the "LP" subscript for the lower polariton coefficients, that we thus note $(u_{c,\mathbf{q}}, u_{x,\mathbf{q}}, v_{c,-\mathbf{q}}, v_{x,-\mathbf{q}})$ in the following sections.

C. Dispersion relations

The eigenvalues of $M_{\mathbf{q}}$ provide the four dispersion relations $\omega_{\{\mathrm{LP,UP};N,G\}}(\mathbf{q})$ and damping rates $\gamma_{\{\mathrm{LP,UP};N,G\}}(\mathbf{q})$ of the Bogoliubov excitations, where labels LP and UP refer to the lower and upper polariton modes, and labels N and G refer to the normal and ghost Bogoliubov excitation branches that exist for each polariton mode, and correspond, respectively, to the positive and negative excitation bands with respect to the condensate energy. Note that LP and UP are still good labels as long as we can neglect their mixing with each other induced by the Bogoliubov transformation, a condition which is well satisfied as long as $\Omega \gg (\mu_s, \mu_{xs})$, as is the case in our experiment [44].

Examples of thus obtained lower polariton normal (dark solid line) and ghost (light solid line) mode dispersion relation are shown in Figs. 1(c) and 1(d) and compared with the free polariton dispersion relation ($\mu_s = \mu_{sx} = 0$, dashed line).

D. Emission intensity $I(\mathbf{q},\omega)$

In order to determine $I(\mathbf{q},\omega)$ we need to evaluate the intracavity photon correlator in Eq. (8). This is achieved by using Eq. (12) and Fourier transforming back to time domain $\hat{a}_{\mathbf{q}}(t) = \int_{-\infty}^{\infty}(d\omega/2\pi)e^{-i\omega t}\hat{a}_{\mathbf{q}}(\omega)$. The relevant term in Eq. (8) is the equation of motion for the intracavity photon operator:

$$\hat{a}_{\mathbf{q}_p+\mathbf{q}}(\omega) = G_{11}\hat{F}_{\mathbf{q}_p+\mathbf{q}}(\omega) + G_{13}\hat{F}^\dagger_{\mathbf{q}_p-\mathbf{q}}(\omega) + (G_{12} - G_{14})[\hat{f}_{\mathbf{q}}(\omega) - \hat{f}^\dagger_{-\mathbf{q}}(\omega)], \tag{19}$$

that involves both the quantum and lattice phonon fluctuations, and where we have set $G(\mathbf{q},\omega) = i[\omega\mathbf{1} - M_{\mathbf{q}}]^{-1}$, and the Langevin forces $\hat{F}$ and $\hat{f}$ are given respectively by the Fourier transforms of Eqs. (16) and (17). We discuss separately the two different fluctuation contributions.

1. Photon-vacuum fluctuations contribution to $I(\mathbf{q},\omega)$

We first focus on the contribution from photon-vacuum fluctuations and calculate $\langle \hat{a}^\dagger_{\mathbf{q}}(\tau)\hat{a}_{\mathbf{q}}(0)\rangle$. Note that this contribution has been derived in a similar way in Ref. [22]. Given that the initial state for the system is the vacuum for the photon modes, only the $\hat{F}^\dagger$ term contributes to the output signal and we find:

$$\langle \hat{a}^\dagger_{\mathbf{q}_p+\mathbf{q}}(\tau)\hat{a}_{\mathbf{q}_p+\mathbf{q}}(0)\rangle_Q = \sum_{k_z} \kappa e^{i\tau\omega^{(\alpha)}_{\mathbf{q}_p-\mathbf{q},k_z}} |G_{13}(\mathbf{q},\omega^{(\alpha)}_{\mathbf{q}_p-\mathbf{q},k_z})|^2. \tag{20}$$

From Eq. (8), we then find the corresponding output signal:

$$I_Q(\mathbf{q}_p+\mathbf{q},\omega) = \gamma^2_{\mathrm{cav}}|G_{13}(\mathbf{q},\omega)|^2/\pi. \tag{21}$$

This expression agrees with that derived in Ref. [22]. The characteristic scattering rate between the condensate photonic fraction and the external photonic vacuum is thus fixed by γ_{cav}, estimated in our experiment to $\gamma_{\mathrm{cav}} \simeq 25$ μeV. $G_{13}(\mathbf{q},\omega)$ can be made explicit using the Bogoliubov transformation Eq. (A50) which leads to

$$I_Q(\mathbf{q}_p+\mathbf{q},\omega) = \gamma^2_{\mathrm{cav}}\left[\frac{|u_{c,\mathbf{q}}v_{c,-\mathbf{q}}|^2/\pi}{(\omega-\omega_{\mathbf{q}_p+\mathbf{q}})^2+\gamma^2_{\mathbf{q}_p+\mathbf{q}}} + \frac{|u_{c,-\mathbf{q}}v_{c,\mathbf{q}}|^2/\pi}{(\omega+\omega_{\mathbf{q}_p-\mathbf{q}})^2+\gamma^2_{\mathbf{q}_p-\mathbf{q}}}\right], \tag{22}$$

for the lower polariton resonance, where we have omitted the LP label. In this expression we have assumed that the normal ($\omega = \omega_{\mathbf{q}_p+\mathbf{q}}$) and ghost ($\omega = -\omega_{\mathbf{q}_p-\mathbf{q}}$) modes are well split in frequency as compared to $\gamma_{\mathbf{q}_p\pm\mathbf{q}}$. In agreement with Ref. [22], we recover the fact that in this regime, the normal branch at $\mathbf{q}_p+\mathbf{q}$ and the ghost branch at $\mathbf{q}_p-\mathbf{q}$ exhibit an equal emission brightness. This property is a fundamental consequence of the fact that in this regime the photons are produced in correlated pairs of $\mathbf{q}_p \pm \mathbf{q}$ momenta via Hamiltonian terms equivalent to $\hat{a}_{\mathbf{q}_p}\hat{a}_{\mathbf{q}_p}\hat{a}^\dagger_{\mathbf{q}_p+\mathbf{q}}\hat{a}^\dagger_{\mathbf{q}_p-\mathbf{q}}$, which destroy two condensate photons (at frequency ω_{las}) to produce a pair of correlated photons in the normal and ghost branches at frequencies $\omega_{\mathrm{las}} \pm \omega$.

2. Phonons' thermal and vacuum fluctuation contribution to $I(\mathbf{q},\omega)$

We now focus on the contribution to the emission intensity originating from coupling to thermal lattice phonons, namely from $\hat{f}_{\mathbf{q}}(\omega) - \hat{f}^\dagger_{-\mathbf{q}}(\omega)$ in Eq. (19). We follow a similar derivation as in the photon-vacuum fluctuations case, using the relation $\hat{f}^\dagger_{-\mathbf{q}}(\omega) = [\hat{f}_{-\mathbf{q}}(-\omega)]^\dagger$. We also use the fact that as v_s, the acoustic speed of sound, is much smaller than the speed of light, the phonons involved in the interaction have a wave vector $k_z \gg |\mathbf{q}|$, so that $\omega = c|k_z|$ and we can replace the $g_{xp}(\mathbf{q},k_z)$ by $g_{xp}(\omega)$. The scattering rate between the condensate excitonic fraction and the phonon vacuum can be written as

$$n_x\gamma_{xp}(\omega) = \pi n_x[g_{xp}(\omega)]^2\rho'_{\mathbf{q},\omega}, \tag{23}$$

with $\rho'_{\mathbf{q},\omega} = \sum_{k_z}\delta(\omega-\omega^{(\mathrm{ph})}_{\mathbf{q},k_z}) = (AL_z)/(2\pi v_s)$ the reduced phonon density of states, where L_z is the quantum well thickness and A a quantization area. An explicit expression of $n_x\gamma_{xp}(\omega)$ as a function of the experimental parameters is given in Appendix A 9. Its maximum value γ^M_{xp} provides an order of magnitude of the exciton-phonon interaction strength, and amounts to $\hbar\gamma^M_{xp} \simeq 5\times10^{-3}$ μeV μm^2 in our experiment. Assuming a density $n_x \sim 5\times10^{10}$ cm^{-2}, it leads to an interaction rate between the condensate excitonic fraction and the phonon vacuum of $\hbar\gamma^M_{xp}n_x \simeq$ 2.5 μeV, which is at about 10 times smaller than $\hbar\gamma_{\mathrm{cav}}$ that determines the scattering rate between the condensate photonic fraction and the photon vacuum. In the generic case where the phonon bath assumes a nonzero temperature, the scattering rate between the condensate excitonic fraction and the phonon thermal bath is enhanced by a thermal phonon population factor, and is given by $n_x\gamma_{xp}(|\omega|)|n_T(\omega)|$, where $n_T(\omega) = 1/[e^{\hbar\omega/(k_BT)}-1]$ is the Bose-Einstein distribution.

We derive the spectral function of elementary fluctuations generated by thermal phonons at any temperature as

$$I_P(\mathbf{q}_p+\mathbf{q},\omega) = \gamma_{\mathrm{cav}}\gamma_{xp}(|\omega|)n_x|n_T(\omega)| \times |G_{12}(\mathbf{q},\omega)-G_{14}(\mathbf{q},\omega)|^2/\pi. \tag{24}$$

As before, we obtain an explicit expression for the matrix elements $G_{12}(\mathbf{q},\omega)-G_{14}(\mathbf{q},\omega)$ using the Bogoliubov transformation [Eq. (A50)]. Within the same assumptions as in the photon-vacuum fluctuations case, we thus obtain for the lower polariton:

$$I_P(\mathbf{q}_p+\mathbf{q},\omega) = \gamma_{\mathrm{cav}}\gamma_{xp}(|\omega|)n_x|n_T(\omega)||u_{x,\mathbf{q}}-v_{x,-\mathbf{q}}|^2 \times\left[\frac{|u_{c,\mathbf{q}}|^2/\pi}{(\omega-\omega_{\mathbf{q}_p+\mathbf{q}})^2+\gamma^2_{\mathbf{q}_p+\mathbf{q}}} + \frac{|v_{c,\mathbf{q}}|^2/\pi}{(\omega+\omega_{\mathbf{q}_p-\mathbf{q}})^2+\gamma^2_{\mathbf{q}_p-\mathbf{q}}}\right]. \tag{25}$$

Note that due to the frequency-dependent factor $\gamma_{xp}(|\omega|)$ as well as to the thermal factor $|n_T(\omega)|$, this line shape is not purely Lorentzian. This aspect turns out to be significant in developing a careful analysis of the experimental data as discussed below.

Equation (25) is an important outcome of our analysis. For the normal mode (first Lorentzian), the output photons are produced via the radiative relaxation of an elementary excitation produced itself by the absorption of a thermal phonon at $(\mathbf{q},\omega)$ by the condensate. These events occur at a rate which is proportional to $\gamma_{xp}(\omega)n_x$, to the thermal population of lattice phonons $n_T(\omega)$, and to the density of

states of the Bogoliubov excitation in the normal mode at $\omega_{\rm las} + \omega$ ($|u_{c,\mathbf{q}}|^2$ factor). For the ghost branch (second Lorentzian), the output photons are produced by radiative relaxation of an elementary excitation produced itself by spontaneous and stimulated emission of a lattice phonon by the condensate [$|n_T(\omega < 0)| = 1 + n_T(-\omega)$ term], where the density of Bogoliubov excitation in the ghost branch is given by the $|v_{c,\mathbf{q}}|^2$ factor. Therefore, in this thermal phonons regime, the two Bogoliubov excitation branches have different intensities. In particular, at $T = 0$ the intensity in the ghost branch does not vanish due to the spontaneous emission of lattice phonons in the phonon vacuum, while the intensity vanishes in the normal branch. This is different from the regime dominated by photon-vacuum fluctuations, and it will turn out to be a key feature to identify in the experiment the physical origin of Bogoliubov excitations.

As will also be discussed more extensively in Sec. IV B, the overall emission rate is also modulated by a $|u_{x,\mathbf{q}} - v_{x,-\mathbf{q}}|^2$ factor, which quantifies the density fluctuation fraction of the excitonic part of a Bogoliubov excitation (the other fraction consisting of phase fluctuation). It is the vanishing of this term for vanishing momenta that leads to a relative decoupling between the condensate and lattice phonons at small $|\mathbf{q}|$.

III. EXPERIMENT

To test these theoretical predictions experimentally, we designed a GaAs-based microcavity in the strong coupling regime containing a single quantum well. This configuration suppresses the dark exciton states that arise in multi-quantum-well structures [45–47], and that contribute an unwanted electronic reservoir that strongly perturbs the Bogoliubov transformation [48,49]. Another contribution to this reservoir is suppressed by choosing a quantum well thicker than usual (17 nm), which results in a narrower excitonic inhomogeneous broadening, and hence to a lower density of states of localized excitons close to resonance with the lower polariton mode [50].

In the experiment, we excite the planar microcavity, with continuous wave (cw) laser light quasiresonant with the zero-momentum state of the lower polariton branch. The upper polariton branch is blueshifted above the LP by a Rabi splitting $\hbar\Omega = 3.28$ meV. By taking advantage of the intentional wedge in the cavity thickness, we choose to address a lower polariton state that has an excitonic fraction of $|X|^2 = 0.53$. This choice offers significant two-body interactions while preserving a narrow spectral linewidth of the LP states. The microcavity temperature (that of lattice phonons) can be tuned between $T_c = 6.6$ and 12 K in the vacuum chamber of a helium flow cryostat. We set the laser frequency at $\omega_{\rm las} = \omega_{\rm LP}(\mathbf{q}_p) + 0.20\ \text{meV}/\hbar$ above our target LP state, where $\omega_{\rm LP}(\mathbf{q})$ is the noninteracting LP dispersion relation and $\hbar\omega_{\rm las} = 1449.0$ meV, and tune its angle close to normal incidence (measured to $\theta_p = 0.1$ deg), which corresponds to a polariton condensate with in-plane momentum $|\mathbf{q}_p| = 0.015\ \mu\text{m}^{-1}$. For both emission and absorption, the extracavity photon incidence angle is related to the in-plane momentum of the corresponding polaritonic state via $|\mathbf{q}| = \omega_{\rm las}\sin(\theta)/c$. Using beam shaping, the laser spot at the microcavity surface (and hence the polariton condensate diameter) amounts to 30 μm, i.e., much larger than the condensate healing length $\xi = \hbar/\sqrt{2m\Delta_{\rm int}} \simeq 1.5\ \mu$m, where $m = 6.6 \times 10^{-35}$ kg is the LP effective mass and $\Delta_{\rm int} \simeq 0.2$ meV is the two-body interaction energy involved in our experiments. A 20-μm-diameter circular spatial filter selects the central part of the condensate, where the condensate density profile is practically constant.

The driven polariton state has a narrow spectral linewidth $\hbar\gamma_{\rm LP}(\theta \sim 0) = \hbar\gamma_0 \simeq 0.03$ meV in the noninteracting regime, as measured after deconvolution of the instrument, such that $\omega_{\rm LP}/\gamma_0 > \sqrt{3}/2$. In this regime, the driven lower polariton condensate intensity $|\psi_{\rm LP}|^2$, and hence the transmitted light intensity $I_t \propto |\psi_{\rm LP}|^2$, exhibits a hysteretic response as a function of the laser intensity I_L [51]. The measured $I_t(I_L)$ is shown in the Supplemental Material (SM), Sec. I [52]. In the high-density state of the bistable region of $I_t(I_L)$, the laser is resonant with the blueshifted LP state and a regime of significant two-body interactions is reached ($\Delta_{\rm int} \geq \hbar\gamma_0$). In the low-density state of the bistability, the laser impinges the low energy tail of the essentially unshifted LP state and the two-body interaction is measured to be 400 times smaller (see SM, Sec. I [52]).

A. Measured spectral function of elementary excitation $I(\theta,\omega)$

1. Noninteracting regime

In order to characterize at best the system parameters which do not depend on interactions, we first tune the laser in the regime of vanishing interactions. The emission of the condensate and its elementary excitations, resolved both in angle (θ) and frequency ($\omega/2\pi$), is collected on the transmission side of the microcavity. The condensate emission intensity I_t, which is peaked at $\omega = \omega_{\rm las}$ and $k = \mathbf{q}_p$, is several orders of magnitude brighter than the spontaneous emission of Bogoliubov excitations $I(\theta, \omega)$; we reject this signal by exploiting the spectrally narrow character of I_t, in using a custom-built image-preserving notch filter of ~0.2 meV bandwidth. Filtering out the very bright condensate signal allows us to measure $I(\theta, \omega)$ for both positive and negative frequency with respect to $\omega_{\rm las}$.

The result is shown in Fig. 2(a) in log (linear) scale for the lower (upper) polariton branch. The emission-free stripe situated between 1448.95 and 1449.2 meV is the result of the above-mentioned filter rejection band. In this noninteracting regime, the elementary excitations have a purely particle (i.e., polaritonic) nature: they correspond to the excitation of a polariton out of the condensate into any other polariton state, including the UP. As expected, we do

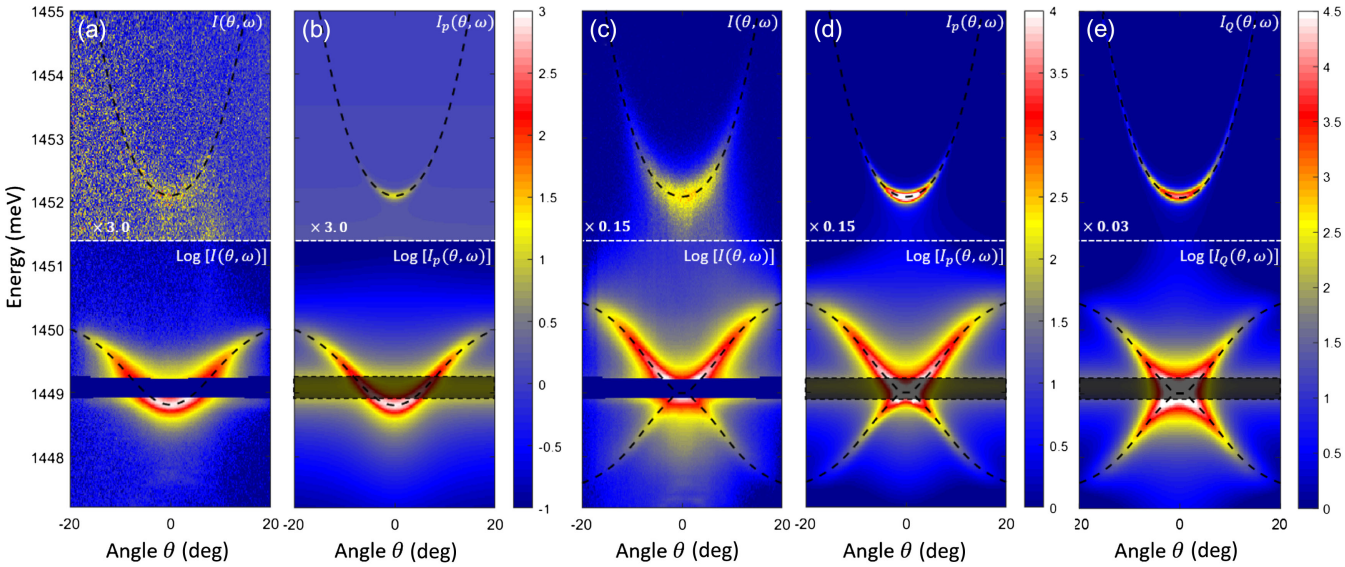

FIG. 2. Measured (a),(c) and theoretical (b),(d),(e) spectral functions $I(\theta,\omega)$ of a resonantly driven polariton condensate in the regime of vanishing interactions (a),(b) and in the interacting regime (c),(d),(e) characterized by $\hbar g_s n_x = 0.19$ meV. The lower polariton spectral area (below the white dashed line) is plotted in log color scale, while the upper area is plotted in a linear color scale with the indicated correction factors. The dashed black line is the theoretical dispersion relation of the Bogoliubov excitations in both situations. The missing blue stripe (a),(c) and gray rectangles (b),(d),(e) show the area rejected from the detection by the spectral filter. In (d) the condensate is assumed to be coupled only to the thermal solid-state phonons with temperature $T_f = 15$ K, as determined from the quantitative analysis of the experiment (see main text). On the contrary, in (e) the elementary excitations are calculated assuming photon-vacuum fluctuations only.

not observe any emission from the ghost mode [at $\omega < \omega_{\mathrm{LP}}(\mathbf{q}_p)$]. Note that the emission of the UP is much dimmer than that of the LP, as expected in an thermally assisted excitation mechanism, as the creation of an upper polariton requires the absorption of a phonon of energy >3.05 meV, while at $T_c = 6$ K the phonon thermal distribution falls off exponentially with the decay constant $k_B T_c = 0.56$ meV. We further elaborate below on the role of thermal phonons in the creation of elementary excitations.

2. Interacting regime

We then increase the laser intensity in order to reach the high-density state of the bistability, where the interactions are significant. In this regime, the interaction energy amounts to $\Delta_{\mathrm{int}} = 0.19$ meV. The measured $I(\theta,\omega)$ is shown in Fig. 2(c). As is immediately apparent, with respect to the noninteracting case [Fig. 2(a)], the interactions modify significantly the elementary excitations dispersion relation. Two different branches can be identified: The one with a positive effective mass and frequency range above ω_{las} is the Bogoliubov excitations normal (N) branch $\hbar\omega_N(\theta)$. The dimmer one, characterized by a negative effective mass, and frequency range below ω_{las}, is the ghost (G) branch $\hbar\omega_G(\theta)$. The shape of $\hbar\omega_{N,G}(\theta)$ is also clearly modified (i.e., steeper) with respect to the free particle dispersion relation $\hbar\omega_{\mathrm{LP}}(\theta)$. These features fully agree with the expected characteristics of the dispersion relation for LP Bogoliubov excitations. Finally, the UP dispersion relation is also clearly visible, and its shape is left essentially unchanged with respect to the noninteracting regime, as we will see more quantitatively later on, and which is expected in the regime where $\Omega \gg \Delta_{\mathrm{int}}$ (see Appendix A 8).

The emission from a ghost branch has been reported once under the intrinsic fluctuations of the system but for a much lower interaction strength [53]. It has also been observed in pump-probe experiments [20,21]. A ghost branch of elementary excitations can also emerge in situations in which the condensate coherence results not from the laser coherence but from spontaneous symmetry breaking [14]. Such condensates have specific fluctuations [54], and their elementary excitations involve a different Bogoliubov-like transformation, characterized by a diffusive Goldstone mode at vanishing frequency [55,56], as well as a ghost mode [57–59].

3. Data analysis

In order to extract the different relevant observables from these measured $I(\theta,\omega)$, such as, in particular, the dispersion relation of the different modes $\omega_j(\theta)$ ($j = \{\mathrm{LP}, \mathrm{UP}\}$ in the noninteracting regime and $j = \{N, G, \mathrm{up}*\}$ in the interacting regime, where UP* labels the normal branch of the upper polariton), as well as the peak-integrated intensity $A_j(\theta)$ of those modes, we first use the measurement in the noninteracting regime carried out at different

temperatures (between $T_c = 6.6$ K and $T_c = 12$ K). From these data, we can precisely determine most experimental parameters such as, e.g., the bare exciton and cavity energies, the Rabi splitting, as well as the cavity photon effective mass. Moving then to the interacting regime, we fit the experimental $I(\theta, \omega)$ using Eq. (24), keeping fixed these parameters that do not depend on interactions, and introduce three additional θ-dependent fit parameters, which allow us to freely capture both the energy and the amplitude of each individual peak in the experiment. As further discussed in the Supplemental Material [52], this method provides us with the experimental values of $\omega_j(\theta)$ and $A_j(\theta)$ that can then be compared with the theory, allowing us to estimate the remaining interaction-dependent parameters of the model.

4. Theoretical spectral functions

In the noninteracting regime, $|v_c|^2 = 0$; from Eq. (22) it follows that the photon-vacuum fluctuations cannot create any elementary excitation, while thermal phonons can. The corresponding theoretical spectral function $I(\theta, \omega)$ is shown in Fig. 2(b) and is in excellent agreement with the measured spectral function [Fig. 2(a)]. In the next section, we will proceed to a quantitative comparison between theory and experiments. We next move to the interacting regime and keep the same model parameters as in the noninteracting case, except for a nonzero value of the nonlinearity $\hbar g_s n_x = 0.19$ meV, and a higher temperature $T = 15$ K $> T_c$. This temperature higher than that of the cryostat is likely the result of residual absorption of the high intracavity field by the GaAs alloy, which produces a heating power due to ensuing nonradiative recombination. By repeating the same analysis as above, namely, assuming only contribution from thermal lattice phonons, yields the theoretical spectral function shown in Fig. 2(d). Also in this case we find an extremely good agreement with the experimental spectral function [Fig. 2(c)]. The assumption of neglecting the photon-vacuum fluctuations will be justified in detail in Sec. III C by the analysis of the spectral intensities.

5. Thermal fluctuations versus photon-vacuum fluctuations

As discussed in Sec. II, the generation of elementary excitations by thermal phonons or by photon-vacuum fluctuations results in a very different $I(\theta, \omega)$ pattern: Figures 2(b) and 2(d) show the calculated spectral functions including only excitations via thermal phonons, while Fig. 2(e) shows the corresponding pattern calculated assuming only quantum photon fluctuations. The reason for this difference is that in the quantum regime, excitations are only created in correlated pairs, implying that—for $\mathbf{q}_p = 0$—$I(\theta, \omega)$ and $I(-\theta, -\omega)$ have an equal brightness. In the regime dominated by thermal lattice phonons, the mechanism generating elementary excitations is not expected to produce as many pair correlations. We notice however that a finite amount of correlations is still expected in this regime, as the lattice phonon which is emitted for the creation of an excitation at $(-\omega, -\theta)$ has precisely the right energy and momentum for the creation, via its absorption, of a second excitation at (ω, θ). A quantitative account for the correlation properties of the spontaneous emission signal, both on the theory and experimental level, exceeds the scope of the present study, but represents a very clear future research direction. In the next sections, we proceed to a quantitative analysis of the experimental data.

B. Dispersion relations $\omega_j(\theta)$

1. Comparison between experiment and theory

From the fitting procedure of the spectral function $I(\theta, \omega)$ as described in the previous section, we extract the experimental dispersion relations of the elementary excitations. In the noninteracting regime, the result is shown in Figs. 3(a) and 3(c) for both the upper $[\omega_{\mathrm{UP}}(\theta)]$ and lower $[\omega_{\mathrm{LP}}(\theta)]$ polariton modes. In the interacting regime, three different modes are extracted: $\omega_G(\theta)$, $\omega_N(\theta)$ [Fig. 3(d)] for, respectively, the ghost and normal modes of the lower polariton and $\omega_{\mathrm{UP}*}(\theta)$ [Fig. 3(b)] which corresponds to the upper polariton branch that retains its free particle character in the limit $\hbar\Omega \gg \Delta_{\mathrm{int}}$ [44]. The theoretical dispersion relations obtained from diagonalizing the $M_{\mathbf{q}}$ matrix Eq. (15) are shown as the solid lines, using the parameters of the "hotter" regime described above, and by adjusting the two coefficients g_s and g_x that describe the interactions in the polariton gas.

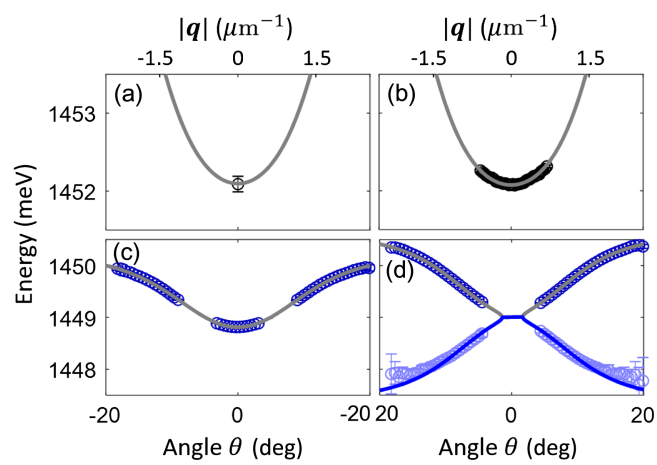

FIG. 3. Dispersion relations in the noninteracting (a),(c) and interacting (b),(d) regime at $T_c = 6.6$ K. The data points extracted from the analysis of the measured spectral functions $I(\theta, \omega)$ are shown in black for the upper polariton branch, in dark (light) blue for the normal (ghost) mode of the lower polariton, with error bars determined from the fitting procedure and corresponding to the 1σ confidence interval. The solid lines show the theory.

We obtain an excellent quantitative agreement between theory and experiment. In particular, the fact that the theory accurately reproduces both (i) the N and G branches spectral blueshift and (ii) the slope of $\omega_{N,G}(\theta)$ at low momenta implies that no additional reservoir is perturbing the Bogoliubov transformation. Indeed, we have shown both experimentally and theoretically in previous works [49,60] that a reservoir of particles much heavier than polaritons (such as, e.g., electron-hole pairs or dark excitons) coexisting with the condensate would induce an additional blueshift $\Delta_{\rm res}$ to the dispersion relation, but would not modify the speed of sound c_s, for which the relation $c_s = \sqrt{\Delta_{\rm int}/m}$ remains valid. Since the experimentally observed blueshift is $\Delta_o = \Delta_{\rm int} + \Delta_{\rm res}$, in the presence of a reservoir, one finds that $c_s < \sqrt{\Delta_o/m}$. Note that this analysis is also valid for nonsonic states, in which the dispersion relation slope is also determined only by $\Delta_{\rm int}$, and thus also leads to a similar inequality when $\Delta_o > \Delta_{\rm int}$, something that can be verified numerically. This analysis thus shows that within the experimental uncertainty, the measured elementary excitations involve no such reservoir.

We note that the best fitted dispersion relation shows a flat segment around $\theta = 0$, which typically indicates the proximity of a dynamical instability. This is consistent with the experiment as, while we do not observe any signature of instability, we indeed operate the system close to an instability point, namely the switch down point of the upper branch of the hysteresis curve (the working point is labeled "3" in Fig. 1 of the Supplemental Material [52]). This working point provides indeed the best compromise between high interaction energy and low laser power. In practice, the onset of instability is determined by the largest eigenvalues' imaginary part becoming positive $\Gamma_{B,m}$ [15]. Our fit yields $\Gamma_{B,m} = +50^{+85}_{-65}$ μeV, which is compatible with stable solutions within the experimental error bars.

2. Excitonic nonlinearity

The best fit obtained above for the dispersion relation in the interacting case involves the ratio $g_x n_x / g_s n_x$ of the nonlinear contributions, where n_x is the excitonic fraction of the condensate density. The fact that all three dispersion relation branches $(G, N, \mathrm{UP}*)$ are experimentally accessible provides us with a unique mean to determine this ratio unambiguously. Indeed, while both g_x and g_s result in a blueshift of the lower polariton N and G modes, g_x would also blueshift the UP* branch with respect to its noninteracting counterpart; on the other hand, g_s leaves this UP* branch spectrally unshifted, and leads to an effectively reduced Rabi splitting. This qualitative difference allows us to clearly separate both g_s and g_x contributions, and yields the ratio $g_x/g_s \simeq 0^{+0.3}_{-0}$, where 0 is the best fit, and $\hbar g_s n_x = 0.19$ meV. This result is of significant interest, and its microscopic interpretation deserves a detailed analysis that exceed the scope of this work.

Let us mention that the fact that g_s seems to dominate over g_x does not contradict previous works dealing with polaritonic nonlinearities, since, as explained above, g_s and g_x contribute to blueshifting the LP mode which is the only focus of nearly all studies on exciton polaritons, while the upper polariton mode is typically disregarded.

C. Emission intensity of elementary excitations

We then extract $A_j(\theta)$ from the measured spectral function $I(\theta, \omega)$, which is defined as the spectral integration of the emission intensity over the peaks of each mode $j = N$, G, as labeled in Eq. (25). $A_j(\theta)$ is the right observable to identify the origin of the fluctuations generating the elementary excitations (namely, thermal lattice phonons or photon-vacuum fluctuations). Assuming narrow Lorentzian line shapes, Eq. (25) yields a simple approximate expression for $A_j(\theta)$ in the regime dominated by thermal lattice phonons that reads:

$$A_N(\theta) \simeq \gamma_{\rm cav}\gamma_{xp}[\omega_N(\theta)]n_x n_T[\omega_N(\theta)]|u_c(\theta)|^2 \times |u_x(\theta) - v_x(\theta)|^2/\gamma_N(\theta), \tag{26}$$

and, similarly,

$$A_G(\theta) \simeq \gamma_{\rm cav}\gamma_{xp}[-\omega_G(\theta)]n_x\{1 + n_T[-\omega_G(\theta)]\}|v_c(\theta)|^2 \times |u_x(\theta) - v_x(\theta)|^2/\gamma_G(\theta), \tag{27}$$

where $-\omega_G(\theta) > 0$ and we assumed that $\mathbf{q}_p \approx 0$. In the regime dominated by photon-vacuum fluctuations, Eq. (22) yields:

$$A_N(\theta) = A_G(\theta) \simeq \gamma_{\rm cav}^2|u_c(\theta)v_c(\theta)|^2/\gamma_N(\theta). \tag{28}$$

In our dataset, the N mode is found much brighter than the G mode, which is in agreement with Eqs. (26) and (27), and not with Eq. (28). This feature rules out a dominant contribution of photon-vacuum fluctuations in this experiment.

The quantitative analysis of $A_j(\theta)$ is shown for a phonon temperature $T_c = 6.6$ K, both in the noninteracting case [Fig. 4(a)] and in the interacting case [Fig. 4(b)]. In the noninteracting case, we observe a decay of $A_{\rm LP}(\theta)$ as a function of θ which is in very good agreement with the theoretical prediction. The latter also agrees quantitatively with the theory in the interacting case assuming $T = 15$ K as explained above. Importantly, the relative intensity between $A_G(\theta)$ and $A_N(\theta)$ is captured strikingly well in this log-scaled plot, except at small angles where $A_G(\theta)$ is found to deviate from the theory. Indeed at smaller angles, the Bogoliubov excitation peaks become increasingly harder to separate from an additional emission contribution that we attribute to spatial inhomogeneities. This agreement shows that the generation of elementary excitations is most likely dominated by thermal phonon in our experimental conditions.

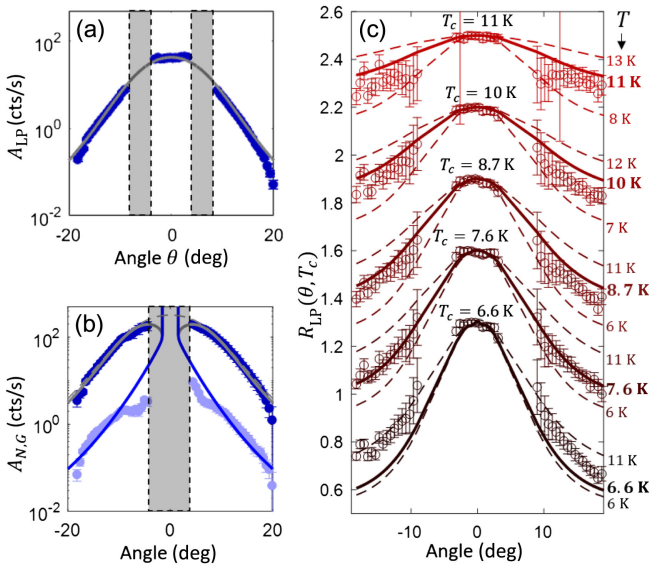

FIG. 4. Analysis of integrated emission intensity $A_j(\theta)$. Measured and theoretical $A_j(\theta)$ at $T_c = 6.6$ K (a) in the noninteracting regime ($j = \mathrm{LP}$) and (b) in the interacting regime, where the normal (ghost) mode $j = N$ ($j = G$) corresponds to the upper (lower) curve of dark (light symbols). The theory is shown as solid lines. The gray rectangle indicates the area of inaccessible measurements due to the spectral filter rejection in the experiment. (c) Measured integrated intensity ratio $R_{\mathrm{LP}}(\theta)[T_c] = A_{\mathrm{LP}}(\theta)[T_c]/A_{\mathrm{LP}}(\theta)[T_c = 12\ \mathrm{K}]$ for $T_c = [7.6, 8.7, 10, 11]$ K (symbols) in the noninteracting regime. The theory assuming the nominal phonon temperature $T = T_c$ is shown as a solid line, as well as two more temperatures: a lower and a higher one with 5 K difference, which are shown as dotted lines. The error bars represent the 1σ confidence interval of the plotted experimental values. They are obtained directly (a),(b) or derived (c) from the integrated intensity 1σ confidence interval provided by the fitting procedure.

We confirm this important feature by analyzing the ratio $R_{\mathrm{LP}}(\theta)[T_c] = A_{\mathrm{LP}}(\theta)[T_c]/A_{\mathrm{LP}}(\theta)[T_0]$ in the noninteracting case, where T_0 is a reference temperature, and $A_{\mathrm{LP}}(\theta)[T_c]$ is the measured lower polariton intensity at another cryostat temperature T_c. According to Eq. (26), $R_{\mathrm{LP}}(\theta)$ is free from any temperature-independent parameters such as the nontrivial energy-dependent exciton-phonon interaction $g_{xp}(\omega)$, that involves the excitonic envelope wave function, and it depends only on temperature as $R_{\mathrm{LP}}(\theta)[T_c] = n_{T_c}(\omega)/n_{T_0}(\omega)$, where $n_{T_c}(\omega)$ is the Bose-Einstein distribution of temperature T_c evaluated at $\omega = \omega_{\mathrm{LP}}(\theta)$. In the experiment, $R_{\mathrm{LP}}(\theta)[T_c]$ is not as simple, as the excitonic transition energy, and to a lesser extent the cavity mode, both redshift for increasing temperature. This redshift modifies the LP dispersion relation $\omega_{\mathrm{LP}}(\theta)$ and the excitonic fraction. However, $R_{\mathrm{LP}}(\theta)$ is still an observable that involves a lower number of complex experimental parameters. We thus perform this analysis varying the cryostat temperature in the range $T_c = [6.6, 7.6, 8.7, 10, 11, 12]$ K, and choose $T_c = 12$ K as the reference temperature T_0. The result is shown in Fig. 4(c) and compared with the theoretical prediction for $R_{\mathrm{LP}}(\theta)[T_c]$ including the temperature-dependent parameters mentioned above. We analyzed the experimental uncertainty [see the dashed lines in Fig. 4(c)] and found that the temperature estimate is accurate within 5 K. Since this accuracy is comparable with the investigated temperature range, a fully quantitative comparison is not possible; however, the observed trend is clearly consistent with a regime dominated by thermal phonons. The two analyses presented in this section thus demonstrate consistently that in our experiment, the Bogoliubov excitations result dominantly from the interaction of the condensate with thermal lattice phonons.

D. Characterization of Bogoliubov amplitudes

1. Intensity ratio and Bogoliubov coefficients

In our experiment, the fact that the Bogoliubov excitations are created dominantly by interaction with the thermal bath of lattice phonons opens up a unique opportunity to obtain a quantitative estimate of the Bogoliubov coefficients $[u_c(\theta), u_x(\theta), v_c(\theta), v_x(\theta)]$, by comparing the emission intensity of the ghost branch and of the normal branch. Indeed, assuming that $\gamma_G(\theta) \simeq \gamma_N(\theta)$, and using the fact that $\mathbf{q}_p \approx 0$, the intensity ratio $R_{GN}(\theta) = A_G(\theta)/A_N(\theta)$ assumes the strikingly simple expression:

$$R_{GN}(\theta) = \frac{|v_c(\theta)|^2}{|u_c(\theta)|^2} e^{\hbar\omega_N(\theta)/k_B T}. \tag{29}$$

Experimentally, A_G and A_N are measured in the exact same experimental conditions, as they are obtained in a single shot of the CCD camera, so that no extra θ-dependent factor remains in the ratio R_{GN}.

The comparison between the experiment carried out at $T_c = 6.6$ K and the corresponding theory is shown in Fig. 5(a). Considering the experimental uncertainty quantified by the error bars (note also that the full range of the plot is only $R_{GN} = [0, 8]\%$), we obtain a fairly good agreement, regarding both the value of the ratio itself and its trend as a function of θ.

In order to illustrate the crucial role of temperature on the brightness of the ghost branch with respect to the normal branch, theoretical plots of $R_{GN}(\theta)$ are shown in Fig. 5(a) for several other temperatures between 6.5 K and ∞ (dashed lines). When the temperature is much higher than the highest frequency of the lower polariton mode [namely, when $k_B T \gg k_B T_{GN} = \hbar\omega_N(\theta_{\max})$, which in our case corresponds to $T_{GN} \simeq 15$ K], we have $R_{GN} \simeq |v_c/u_c|^2$ [dashed line labeled as $T = \infty$ in Fig. 5(a)]. Upon cooling down below T_{GN}, fewer thermal phonons are available to create excitations into the normal branch (starting with the highest energy states, namely largest angles or momenta), so that the ghost branch, which is populated by both spontaneous and stimulated emission of lattice phonons, increases in intensity with respect to the normal branch.

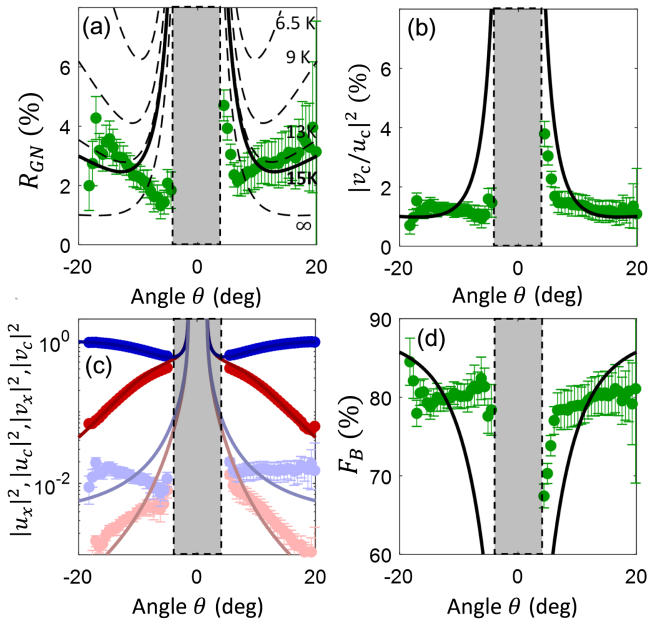

FIG. 5. Bogoliubov amplitudes analysis. (a) $R_{GN}(\theta)$, (b) photonic Bogoliubov squared amplitude ratio $|v_c(\theta)/u_c(\theta)|^2$. The four squared Bogoliubov amplitudes are plotted in (c) in semilog scale with u_c (v_c) in dark (light) blue and u_X (v_X) in dark (light) red. (d) Measured and theoretical Bogoliubov correction factor $F_B(\theta)$ to the polariton-phonon interaction rate. The data points in (a),(b),(d) are shown in green. In all panels, the solid lines show the theory. The dashed line in (b) shows the theoretical $R_{GN}(\theta)$ assuming the different phononic temperatures indicated, in addition to the best fit $T = 15$ K, which is shown as a solid line. The gray rectangle indicates the area of inaccessible measurements due to the spectral filter rejection in the experiment. All the error bars correspond to the 1σ confidence interval of the plotted experimental values and are derived from the 1σ confidence interval of the integrated intensity obtained directly in the fitting procedure.

Remarkably, one predicts that for low enough temperature, and neglecting the photon-vacuum fluctuations to get a simple estimate, the ghost branch emission intensity can even overcome that of the normal branch. For a given θ, this happens when $R_{GN}(\theta) \geq 1$, namely when $k_B T \leq \hbar\omega_N / \log(|u_c/v_c|^2)$. For instance, using our experimental parameters and a typical angle $\theta = 10$ deg, we find that the temperature for which equal brightness of the two branches is achieved is $T_{\mathrm{EB}} \lesssim 5.2$ K, which is about 3 times colder than the actual phonon temperature estimated for this experiment. This criterion provides a likely explanation regarding the notoriously difficult observation of the ghost mode spontaneous emission in exciton-polariton systems, in addition to the requirement of eliminating any detrimental electronic reservoir.

Finally, it is straightforward to estimate the Bogoliubov coefficient ratio $|v_c/u_c|^2 = R_{GN} \exp[-E_N/k_B T]$ from $R_{GN}(\theta)$, using the temperature $T = 15$ K. The result is shown in Fig. 5(b) together with the theory (solid line). In full agreement with the theory, we find that the photonic fraction of the "hole" character of Bogoliubov excitations ($|v_c|^2$) amounts to ~1.5% at high angle, and up to ~4% for the lowest angles. While this correlation is modest, it is clearly established in our experiment, and the detailed understanding provided by our theoretical model is a guide toward realizing more strongly correlated quantum fluids of light, and, in particular, generating quantum-correlated pairs of excitations by lowering the temperature to enter a regime dominated by photon-vacuum fluctuations (see Sec. IV A).

2. *Extracting all Bogoliubov coefficients*

The Bogoliubov transformation is defined by four complex coefficients (u_c, u_x, v_c, v_x), that characterize the exciton and photon particle fractions (first two) and the exciton and photon hole fractions (last two), of a Bogoliubov excitation [see Sec. II. B and Eq. (A50)]. In our experimental conditions, these four amplitudes can be determined to within a good approximation from the knowledge of the ratio $|v_c/u_c|^2$ determined above, and from the knowledge of the excitonic X and photonic C Hopfield coefficients of the (noninteracting) polariton states [their $\mathbf{q}$ dependence has been dropped like for (u, v)]. Indeed, as mentioned earlier, the fact that the Rabi splitting is much larger than the interaction energy (namely, $\Omega \gg \Delta_{\mathrm{int}}$) implies that the lower and upper polaritons do not hybridize under the Bogoliubov transformation, and that the hole fraction of the upper polaritons is vanishing [44]. One can thus define two lower-polariton-only Bogoliubov coefficients (u, v) that are related to the four original coefficients via the relations $(u_x, v_x)/X = (u_c, v_c)/C = (u, v)$, which leads also to $|v_c/u_c|^2 = |v/u|^2$ (see Appendix A 8 for a detailed derivation). In this regime, the Bogoliubov coefficients are approximately real, and using the normalization condition $|u|^2 - |v|^2 = 1$, one can thus derive both u and v from the knowledge of $|v_c/u_c|^2$, and hence all four coefficients (u_c, u_x, v_c, v_x). By doing so, one obtains all the Bogoliubov coefficients plotted in Fig. 5(d), together with their exact theoretical prediction showing a remarkable agreement that further supports the approximations discussed above.

IV. DISCUSSION

A. Crossover temperature into the regime dominated by photon-vacuum fluctuations

Owing to the thermal population factor entering the interaction between the condensate and the lattice phonons [$n_T(\omega)$ in Eq. (25)], the relative contribution of photon-vacuum fluctuations and of the lattice phonons can be tuned to a large extent by changing the lattice temperature T. Within the right parameters range, a nonzero crossover temperature can thus be determined, below which the Bogoliubov excitations emission results dominantly from

the interaction between the condensate and the photon-vacuum fluctuations. In such a regime, the condensate starts to effectively decouple from the lattice, which is most likely a necessary condition for the elementary excitations to generate quantum correlations [22–27,61]. A quantitative derivation of their emergence would require calculating two-photon correlations [22], which exceeds the scope of this work.

As we shall see in this section, a single crossover temperature cannot be defined for the whole condensate. The highest crossover temperature occurs for low-momenta excitations, and gets lower for higher momenta. Upon cooling down, the condensate decoupling from the lattice is thus a smooth process, in which an increasing range of momenta (or equivalently of emission angle θ) of Bogoliubov excitations becomes more coupled to the photon-vacuum fluctuations than to the lattice.

The crossover temperature can be simply estimated for the normal branch by equating Eqs. (26) and (28), yielding

$$T_N^{(\mathrm{cr})}(\theta) = \frac{\hbar\omega_N(\theta)/k_B}{\log\left[1 + \frac{\gamma_{xp}(\theta)n_x}{\gamma_{\mathrm{cav}}}\frac{|u_x(\theta)-v_x(\theta)|^2}{|v_c(\theta)|^2}\right]}. \tag{30}$$

Similarly, for the ghost mode we equate Eqs. (27) and (28) to obtain

$$T_G^{(\mathrm{cr})}(\theta) = -\frac{\hbar\omega_N(\theta)/k_B}{\log\left[1 - \frac{\gamma_{xp}(\theta)n_x}{\gamma_{\mathrm{cav}}}\frac{|u_x(\theta)-v_x(\theta)|^2}{|u_c(\theta)|^2}\right]}. \tag{31}$$

One difficulty in deriving a quantitative estimate of $T_{N,G}^{(\mathrm{cr})}(\theta)$ is that it requires knowing the excitonic density n_x involved in the condensate, which is not easy to determine in the experiment. However, note that $T_{N,G}^{(\mathrm{cr})}(\theta)$ depends only logarithmically (and hence weakly) on the product $\gamma_{xp}(\theta)n_x$. Regarding n_x, we use the fact that it is necessarily lower than the excitonic Mott density $n_{x,M}$, for which the Rabi splitting, and hence the polaritonic state, would be fully collapsed. $n_{x,M}$ depends only on the excitonic Bohr radius as $n_{x,M} \sim 1/(\pi a_B^2)$ and is thus easy to estimate; it amounts to $\simeq 3.2 \times 10^{11}$ cm^{-2} in our quantum well. Concerning $\gamma_{xp}(\theta)$, a realistic estimate is derived in Appendix A 9.

The resulting crossover temperature for the normal branch $T_N^{(\mathrm{cr})}(\theta)$ is thus plotted in Fig. 6(a), by considering a range of excitonic densities between 5% (lightest gray line) and 100% (red line) of $n_{x,M}$. The parameters used in the calculation are those derived for our experiment at $T_c = 6.6$ K, and the total blueshift $\hbar g_s n_x = 0.19$ meV is kept constant (and hence the Bogolibuov coefficients as well) to its measured value. This analysis shows that the normal branch crossover temperature is situated realistically within the interval [2.5, 4.5] K within a typical emission angular aperture of 10 deg.

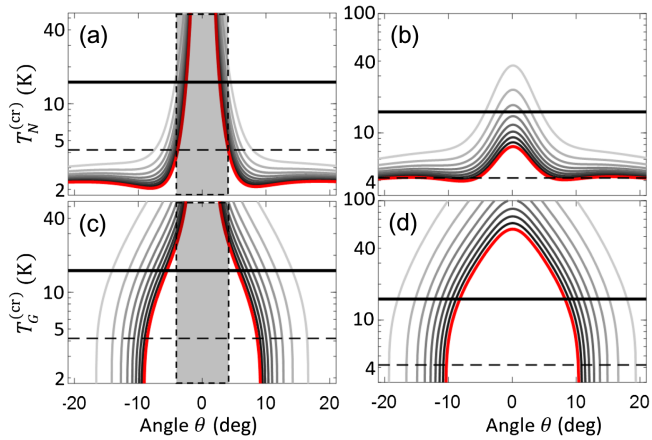

FIG. 6. Calculated angle-dependent thermal to quantum regime crossover temperature $T_{\mathrm{cr},N}$ for the normal (a) and $T_{\mathrm{cr},G}$ for the ghost (c) modes in semilog scale. The excitonic density is increasing from $n_x = 0.1n_{x,M}$ to $n_x = 0.9n_{x,M}$ from the lightest to the darkest gray lines. The thick red line shows the result assuming $n_x = n_{x,M}$, the Mott density, which constitutes a solid upper bound of n_x. The thick horizontal line shows a photon temperature of $T_c = 15$ K, and the dashed horizontal line shows liquid helium temperature $T_{\mathrm{He}} = 4.2$ K. Panels (a) and (c) are calculated for the total blueshift achieved in this work $\hbar g_s n_x = 0.19$ meV, while panels (b) and (d) are calculated for a twice larger blueshift $\hbar g_s n_x = 0.38$ meV.

The ghost branch crossover temperature $T_G^{(\mathrm{cr})}(\theta)$ is shown in Fig. 6(c). As an obvious difference with the normal branch, no crossover temperature can be determined above a critical angle ($|\theta_{\mathrm{cr}}| \sim 10$ deg in our simulation of this experiment), because above $|\theta_{\mathrm{cr}}|$, the photon-vacuum fluctuations cannot overcome the vacuum fluctuations of the lattice phonons that are present at $T = 0$ K, for the generation of Bogoliubov excitations. This feature is particularly striking as it means that in this realistic case the condensate can never be considered decoupled from its solid-state lattice environment for all possible elementary excitations momenta. Physically, the generation of Bogoliubov excitations by the lattice at $T = 0$ K occurs into the ghost mode by spontaneous emission of phonons into the phonon vacuum. The corresponding $T = 0$ K ghost branch emission intensity $A_{G,0}$ can be derived from Eq. (27) as

$$A_{G,0} = A_G(\theta, T = 0) = \gamma_{\mathrm{cav}}\gamma_{xp}(\theta)n_x \times |v_c(\theta)|^2|u_x(\theta) - v_x(\theta)|^2. \tag{32}$$

When $A_{G,0}$ is larger than that the contribution generated by photon-vacuum fluctuations [Eq. (28)], the latter can then never become dominant for the ghost branch. The parameters involved in $A_{G,0}$ show that $|\theta_{\mathrm{cr}}|$ can be increased via different parameters such as the total interaction energy, or the excitonic $|X|^2$ and photonic $|C|^2$ fractions [embedded within the Bogoliubov coefficients (u_x, v_x, u_c, v_c)] that allow modulating to a large extent the relative coupling of

polaritons to phonons, on one hand ($\propto |X|^2$), and to free space photons ($\propto |C|^2$), on the other hand.

In Figs. 6(b)–6(d), we computed the crossover temperature $T_N^{(\mathrm{cr})}(\theta)$ and $T_G^{(\mathrm{cr})}(\theta)$ for the same range of excitonic densities but considering a twice larger total blueshift $\hbar g_s n_x = 0.38$ meV. This change amounts to increasing the laser intensity substantially and hence changing the working point on the hysteresis curve (Fig. 1 of the SM [52]) to the right, where the elementary excitations exhibit a gaped dispersion relation. The benefit of this increase of interaction energy is twofold: the $|v_{x,c}|^2$ coefficient magnitude increases, and the spectral gap in the excitation dispersion relation is of comparable size as the spectral filter in the experiment. As a result, the emission even from the smallest angles, where $|v_{x,c}|^2$ is the largest, becomes experimentally accessible. Note that in practice, increasing the excitonic fraction $|X|^2$ or the laser intensity typically require specific optimization, as it results in spectral broadening of the polariton state and/or in an increased heating due to residual absorption.

B. Decoupling of low-momenta Bogoliubov excitations from lattice phonons

One last striking property that we examine in this section is the overall reduction of the coupling strength between polaritons and the thermal bath of lattice phonons that results from the Bogoliubov transformation. This reduction can be seen already at the Hamiltonian level in which rewriting the exciton-phonon interaction term [Eq. (11)] in the Bogoliubov basis results in a correction of the interaction energy amplitude $g_{xp}(\omega)$ by a factor $(u_{x,\mathbf{q}} - v_{x,-\mathbf{q}})$. Assuming an LP-only condensate, which as discussed both in Sec. III D and in Appendix A 8 is an excellent approximation in our experiment, this correction factor takes the simpler expression $X_{\mathbf{q}}(u_{\mathbf{q}} - v_{-\mathbf{q}})$ with (u, v) the Bogoliubov amplitudes in the LP basis, and $X_{\mathbf{q}}$ is the usual (noninteracting) LP excitonic Hopfield coefficient. As a result, the phonon-condensate coupling rate which is proportional to $g_{xp}(\omega)^2$ ends up corrected by the factor $F_B = |u_{\mathbf{q}} - v_{-\mathbf{q}}|^2 \leq 1$ by the Bogoliubov transformation of the elementary excitations.

Physically, $|u_{x,\mathbf{q}} - v_{x,-\mathbf{q}}|^2$ actually quantifies the fraction of excitonic density fluctuations in a Bogoliubov excitation, through which polaritons indeed couple to lattice deformations. Remarkably, for small momenta $|u_{x,\mathbf{q}} - v_{x,-\mathbf{q}}|^2 \ll 1$, and therefore the corresponding Bogoliubov excitations become effectively decoupled from the bath of thermal lattice phonons. This phenomenon is somewhat reminiscent of a superfluid behavior, in which, as a consequence of interparticle interactions, the system effectively decouples from slowly moving defects. In the context of reaching the regime dominated by photon-vacuum fluctuations, this decoupling favors its emergence in low-momenta states, and thus increases the crossover temperature into the quantum regime as already pointed our in the previous section [cf. Eqs. (30) and (31)].

Interestingly, we can derive a measurement of $F_B(\theta)$ from our experimental determination of $|v(\theta)/u(\theta)|^2$ presented in Sec. III D as $F_B^2 = (1 - |v/u|)/(1 + |v/u|)$. The result is plotted in Fig. 5(c) alongside the theoretical $F_B = |u_{x,\mathbf{q}} - v_{x,-\mathbf{q}}|^2/X^2$. A Bogoliubov correction factor of $F_B \simeq 80\%$ is found at large angle and decreases to about 70% at lower angles (for the data points which are the closest to the spectral filter), a trend which is in fair agreement with the theory, with deviations mostly coming from the weaker measured emission intensity of the ghost branch at low angles as compared to the theory.

The dataset presented in Fig. 5(d) suggests the onset of a dipping behavior of $F_B(\theta)$ at low angle with respect to higher angles. This dipping is an unambiguous signature of the Bogoliubov-mediated thermal protection mechanism from the phonon bath.

V. CONCLUSION

In this work we have shown that, in general, a quantum fluid of polaritons embedded within a solid-state lattice has strongly modified characteristics and unique properties as compared to the same system considered in vacuum, or to a closed equilibrium system like ultracold atoms. Indeed, the open character of the system implies that the condensate interacts with the fluctuations of its surrounding environment. The environment constituted by the photon vacuum has been well investigated over the past decade and shown to lead to striking properties that remain entirely relevant, such as the fact that this coupling produces a steady-state flux of Bogoliubov excitations, and that their subsequent emission is characterized by pairwise quantum correlations.

This work shows that the vibrating lattice that the condensate is embedded in constitutes a second environment that the condensate is coupled to. We show that it also produces a steady-state flux of Bogoliubov excitations, albeit with a very different spectral function, and a nontrivial lattice-temperature dependence. Strikingly, we predict a nonzero flux of elementary excitations even for a lattice temperature of $T = 0$ K.

We achieve a quantitative understanding of this contribution to the fundamental steady-state flux of elementary excitations via a quantitative comparison between experiment and theory. Our analysis shows in particular that in typical experimental conditions and temperatures, this fundamental steady-state flux is predominantly driven by thermal phonon fluctuations rather than by photon-vacuum fluctuations. This is an obstacle if one wants to explore quantum correlations within the Bogoliubov excitation spectrum, which emerge when the Bogoliubov excitations are driven by photon-vacuum fluctuations. Using our theoretical analysis, we propose realistic experimental strategies to overcome this difficulty in future experiments.

We also highlight a thermodynamical phenomenon by which the Bogoliubov transformation taking place within the quantum fluid reduces its coupling to the thermal bath of lattice phonons, and hence the amount of thermal energy that the condensate absorbs per unit of time in its steady state. This thermal protection mechanism shows up in the steady state in our system owing to its driven-dissipative nature. In equilibrium systems such as ultracold atoms, similar effects have been rather observed in the cooling or heating dynamics, in particular when the role of the heat bath is provided by impurities [62,63] or by another species in the context of a two-components mixture [64–67], such that the heat transfers are governed by an inelastic scattering mechanism similar to that of our exciton-phonon interaction Eq. (6).

ACKNOWLEDGMENTS

The authors wish to thank Iacopo Carusotto for insightful discussions. I. F. acknowledges support from the European Union Horizon's 2020 research and innovation programme under the Marie Sklodowska Curie Grant Agreement No. 101031549 (QuoMoDys). This work was partly supported by the Paris Ile de France Région in the framework of DIM SIRTEQ, by the RENATECH network and the General Council of Essonne, by the European Research Council under the European Union's Horizon H2020 research and innovation programme (StG ARQADIA, Grant Agreement No. 949730), by the European Union (ERC, AdG ANAPOLIS, Grant Agreement No. 101054448), and by the Centre of Quantum Technologies's Exploratory Initiative programme. A. V. acknowledges the European Union's Horizon 2020 research and innovation programme under the Marie Sklodowska-Curie Grant Agreement No. 754303, and under the European Research Council (CoG LATIS, Grant Agreement No. 101044957).

APPENDIX A: DETAILS ON THE THEORETICAL MODEL

1. Input-output formalism

In the experiment, we measure the emission intensity resolved in both frequency and wave vector, denoted as $I(\mathbf{q},\omega)$, where $\mathbf{q}=(q_x,q_y)$ is the in-plane momentum. In order to compute it from the microscopic model, we adopt an input-output formalism. We work in the Heisenberg picture and make the standard assumption that the state is factorized at initial time $t=t_0$, namely, $\hat{\rho}_0=\hat{\rho}_p\otimes|0_{\mathrm{phot}}\rangle\langle 0_{\mathrm{phot}}|$, with $\hat{\rho}_p$ the intracavity polaritonic density matrix and $|0_{\mathrm{phot}}\rangle$ the vacuum for the extracavity photon modes. The latter is an excellent approximation in our experiment, as the typical frequencies involved ($\omega\sim 1.5$ eV) in the problem correspond to a temperature $T>10^4\ \mathrm{K}\gg T_c$, with $T_c\sim 10$ K the cryostat temperature, so that the extracavity modes can be safely considered in a vacuum state. We work in the Markovian approximation in which the bath retains no memory of its interaction with the system.

After a time interval $\Delta t=t-t_0$, the extacavity photon mode at $(\mathbf{q},k_z)$ contains a number of output photons given by $n(\mathbf{q},k_z,\Delta t)=\langle\hat{\alpha}^\dagger_{\mathbf{q},k_z}(t_0+\Delta t)\hat{\alpha}_{\mathbf{q},k_z}(t_0+\Delta t)\rangle$, where the average is taken over the initial state, namely, $\langle\cdots\rangle=\mathrm{Tr}[\hat{\rho}_0\ldots]$. As per the experimental condition, the system is in its steady state, so that this quantity does not depend on the initial time t_0. Experimentally, we measure the photon flux, per unit momentum and frequency, tunneling outside of the microcavity during a time interval Δt, which is macroscopic as compared to the system microscopic timescales; namely,

$$I(\mathbf{q},\omega)=\rho(\mathbf{q},\omega)\lim_{\Delta t\to\infty}\left[\frac{n[\mathbf{q},k_z(\mathbf{q},\omega),\Delta t]}{\Delta t}\right],\quad\text{(A1)}$$

where $\rho(\mathbf{q},\omega)=\sum_{k_z}\delta(\omega-\omega^{(\alpha)}_{\mathbf{q},k_z})$ is the partial density of states of extracavity photons, and $k_z(\mathbf{q},\omega)=\sqrt{\omega^2/c^2-\mathbf{q}^2}$.

Using Heisenberg equations of motion (EOM) for the extracavity photons $i\hbar\partial_t\hat{\alpha}_{\mathbf{q},k_z}=[\hat{\alpha}_{\mathbf{q},k_z}(t),\hat{\mathcal{V}}_{\mathrm{out}}]$, where $\hat{\mathcal{V}}_{\mathrm{out}}$ is given in Eq. (7) in the main text, we can relate their dynamics evolution to the dynamics of intracavity photons

$$\hat{\alpha}_{\mathbf{q},k_z}(t)=e^{-i\omega^{(\alpha)}_{\mathbf{q},k_z}(t-t_0)}\hat{\alpha}_{\mathbf{q},k_z}(t_0)-i\kappa_{\mathbf{q},k_z}\int_{t_0}^{t}dt'e^{-i\omega^{(\alpha)}_{\mathbf{q},k_z}(t-t')}\hat{a}_{\mathbf{q}}(t').\quad\text{(A2)}$$

Since the photonic input state is the vacuum, only the second term in Eq. (A2) contributes to the output signal, leading to

$$I(\mathbf{q},\omega)=\lim_{\Delta t\to\infty}\frac{\gamma_{\mathrm{cav}}}{\pi\Delta t}\int_{t_0}^{t_0+\Delta t}dt_2\int_{t_0}^{t_0+\Delta t}dt_1\times e^{-i\omega(t_2-t_1)}\langle\hat{a}^\dagger_{\mathbf{q}}(t_2)\hat{a}_{\mathbf{q}}(t_1)\rangle,\quad\text{(A3)}$$

with the cavity loss rate $\gamma_{\mathrm{cav}}=\pi\rho(\mathbf{q},\omega)\kappa^2_{\mathbf{q},k_z(\mathbf{q},\omega)}$. Equation (A3) thus shows that the photon emission intensity into the extracavity medium corresponds to the Fourier transform of the two-times correlations $\langle\hat{a}^\dagger_{\mathbf{q}}(t_2)\hat{a}_{\mathbf{q}}(t_1)\rangle$ of the intracavity photons, and hence of the polaritons. We further assume that Δt is much larger than the inverse typical frequency range (namely, $\Delta t\gg 10^{-11}$ s for frequencies in the meV range), allowing us to send $\Delta t\to\infty$. In the steady state, correlation functions depend only on the time difference $\tau=t_2-t_1$, and the output signal simplifies to

$$I(\mathbf{q},\omega)=\frac{\gamma_{\mathrm{cav}}}{\pi}\int_{-\infty}^{+\infty}d\tau e^{-i\omega\tau}\langle\hat{a}^\dagger_{\mathbf{q}}(\tau)\hat{a}_{\mathbf{q}}(0)\rangle;\quad\text{(A4)}$$

namely, it is proportional to the spectral function of the photonic component of the lower polaritons inside of the cavity.

2. Solution of the mean-field steady-state equations

We provide here the details of the solution of Eqs. (9) and (10). Without loss of generality, we can take $\psi_x = \sqrt{n_x}$ and $\psi_c = \sqrt{n_c}e^{-i\phi}$. Experimentally, we control the pump intensity $|F_p|^2$, and n_x, n_c, ϕ spontaneously take their steady-state values, but for the sake of deriving the solutions of the mean-field equations, we take n_x as a parameter, and derive $n_c, \phi, |F_p|^2$ as a function of n_x. First, taking the real and imaginary parts of Eq. (9), we derive the relations:

$$(3g_s n_x/2 - \Omega/2)\sqrt{n_c}\cos\phi = \sqrt{n_x}(\omega_x + g_x n_x), \quad \text{(A5)}$$

$$(g_s n_x/2 - \Omega/2)\sqrt{n_c}\sin\phi = -\sqrt{n_x}\gamma_x/2. \quad \text{(A6)}$$

Taking the square of these relations, and using $\cos^2\phi + \sin^2\phi = 1$, we obtain the ratio:

$$Q_n := \frac{n_c}{n_x} = \frac{(\omega_x + g_x n_x)^2}{(\Omega/2 - 3g_s n_x/2)^2} + \frac{(\gamma_x/2)^2}{(\Omega/2 - g_s n_x/2)^2}. \quad \text{(A7)}$$

This relation gives n_c as a function of n_x. Inserting Q_n into Eqs. (A5) and (A6), we then find the relative phase ϕ as follows:

$$\cos\phi = \frac{\omega_x + g_x n_x}{\sqrt{Q_n}(3g_s n_x/2 - \Omega/2)}, \quad \text{(A8)}$$

$$\sin\phi = \frac{\gamma_x/2}{\sqrt{Q_n}(\Omega/2 - g_s n_x/2)}. \quad \text{(A9)}$$

In our experiment, $\Omega = 3.28$ meV is much larger than $g_s n_x = 0.19$ meV, such that $\cos\phi < 0$ and $\sin\phi > 0$. Using also $g_x n_x = 0$ yields $\tan\phi \simeq \gamma_x/\omega_x(1/2 - g_s n_x/\Omega)$, where $\gamma_x \sim 0.15$ meV and $\omega_x = 1.355$ meV$/\hbar$ (we remind that the frequencies are expressed in the frame rotating at the laser frequency). We see that as long as $g_s n_x/\Omega \ll 1$, $\phi \simeq \pi$, where $\phi = \pi$ is the nominal phase difference in the linear regime for lower polariton states. Once ϕ and n_c are obtained, we finally use Eq. (10) to find $|F_p|^2$:

$$|F_p|^2 = |(\omega_c - i\gamma_{\text{cav}}/2)\sqrt{n_c}e^{-i\phi} + (\Omega/2 - g_s n_x/2)\sqrt{n_x}|^2. \quad \text{(A10)}$$

This provides the solution to the mean-field steady-state equations of the condensate.

3. Polariton interactions in the Bogoliubov approximation

Here, we give the detailed expression for the polariton interaction terms in the Bogoliubov approximation. For the exciton-exciton interaction, it results in

$$\hat{\mathcal{V}}_{xx} = (\hbar g_x n_x/2)\sum_{\mathbf{q}}[\hat{b}^\dagger_{\mathbf{q}_p+\mathbf{q}}\hat{b}^\dagger_{\mathbf{q}_p-\mathbf{q}} + 4\hat{b}^\dagger_{\mathbf{q}_p+\mathbf{q}}\hat{b}_{\mathbf{q}_p+\mathbf{q}} + \hat{b}_{\mathbf{q}_p+\mathbf{q}}\hat{b}_{\mathbf{q}_p-\mathbf{q}}], \quad \text{(A11)}$$

and for the saturation term:

$$\begin{aligned}\hat{\mathcal{V}}_{\text{sat}} = -(\hbar g_s/2)\sum_{\mathbf{q}}\big(&n_x[\hat{a}^\dagger_{\mathbf{q}_p+\mathbf{q}}\hat{b}^\dagger_{\mathbf{q}_p-\mathbf{q}} + 2\hat{a}^\dagger_{\mathbf{q}_p+\mathbf{q}}\hat{b}_{\mathbf{q}_p+\mathbf{q}} \\ &+ \hat{a}_{\mathbf{q}_p+\mathbf{q}}\hat{b}_{\mathbf{q}_p-\mathbf{q}} + 2\hat{a}_{\mathbf{q}_p+\mathbf{q}}\hat{b}^\dagger_{\mathbf{q}_p+\mathbf{q}}] \\ &+ \sqrt{n_c n_x}[e^{-i\phi}\hat{b}^\dagger_{\mathbf{q}_p+\mathbf{q}}\hat{b}^\dagger_{\mathbf{q}_p-\mathbf{q}} + (4\cos\phi)\hat{b}^\dagger_{\mathbf{q}_p+\mathbf{q}}\hat{b}_{\mathbf{q}_p+\mathbf{q}} \\ &+ e^{i\phi}\hat{b}_{\mathbf{q}_p+\mathbf{q}}\hat{b}_{\mathbf{q}_p-\mathbf{q}}]\big),\end{aligned} \quad \text{(A12)}$$

where ϕ is the relative phase between the excitonic and photonic condensate fields.

4. Equations of motion for cavity photons

The EOM for the cavity photons $\partial_t\hat{a}_{\mathbf{q}_p+\mathbf{q}} = (-i/\hbar)[\hat{a}_{\mathbf{q}_p+\mathbf{q}}(t), \hat{\mathcal{H}}_{\text{tot}}]$ is made of three terms. A first term contains the free part and the interaction between cavity photons and excitons [Eq. (2)],

$$-\frac{i}{\hbar}[\hat{a}_{\mathbf{q}_p+\mathbf{q}}, \hat{\mathcal{H}}^{(0)}_{\text{pol}}] = -i\omega^{(0)}_{c,\mathbf{q}_p+\mathbf{q}}\hat{a}_{\mathbf{q}_p+\mathbf{q}} - i\frac{\Omega}{2}\hat{b}_{\mathbf{q}_p+\mathbf{q}}; \quad \text{(A13)}$$

a second term comes from the excitonic saturation mechanism [treated in the Bogoliubov approximation, as explained in the main text, Eq. (A12)],

$$-\frac{i}{\hbar}[\hat{a}_{\mathbf{q}_p+\mathbf{q}}, \hat{\mathcal{V}}_{\text{sat}}] = i(g_s n_x/2)(\hat{b}^\dagger_{\mathbf{q}_p-\mathbf{q}} + 2\hat{b}_{\mathbf{q}_p+\mathbf{q}}); \quad \text{(A14)}$$

and a third term contains the coupling to extracavity photons [Eq. (7)],

$$-\frac{i}{\hbar}[\hat{a}_{\mathbf{q}}, \hat{\mathcal{V}}_{\text{out}}] = -i\sum_{k_z}\kappa_{\mathbf{q},k_z}\hat{\alpha}_{\mathbf{q},k_z}. \quad \text{(A15)}$$

5. Equations of motion for quantum well excitons

The EOM for the quantum well excitons $\partial_t\hat{b}_{\mathbf{q}_p+\mathbf{q}} = (-i/\hbar)[\hat{b}_{\mathbf{q}_p+\mathbf{q}}(t), \hat{\mathcal{H}}_{\text{tot}}]$ is made of three terms. A first term contains the free part and Rabi coupling to cavity photons,

$$-\frac{i}{\hbar}[\hat{b}_{\mathbf{q}_p+\mathbf{q}}, \hat{\mathcal{H}}^{(0)}_{\text{pol}}] = -i\omega^{(0)}_{x,\mathbf{q}_p+\mathbf{q}}\hat{b}_{\mathbf{q}_p+\mathbf{q}} - i\frac{\Omega}{2}\hat{a}_{\mathbf{q}_p+\mathbf{q}}; \quad \text{(A16)}$$

a second term comes from the excitonic saturation and Coulomb interactions [treated in the Bogoliubov approximation, Eqs. (A12) and (A11)],

$$-\frac{i}{\hbar}[\hat{b}_{\mathbf{q}_p+\mathbf{q}}, \hat{\mathcal{V}}_{\mathrm{sat}} + \hat{\mathcal{V}}_{xx}] = i(g_s n_x/2)(\hat{a}^\dagger_{\mathbf{q}_p-\mathbf{q}} + 2\hat{a}_{\mathbf{q}_p+\mathbf{q}}) + ig_s\sqrt{n_x n_x}[e^{-i\phi}\hat{b}^\dagger_{\mathbf{q}_p-\mathbf{q}} + (2\cos\phi)\hat{b}_{\mathbf{q}_p+\mathbf{q}}] - ig_x n_x(\hat{b}^\dagger_{\mathbf{q}_p-\mathbf{q}} + 2\hat{b}_{\mathbf{q}_p+\mathbf{q}}); \tag{A17}$$

and a third term comes from the coupling to lattice phonons [in the Bogoliubov approximation, Eq. (11)],

$$-\frac{i}{\hbar}[\hat{b}_{\mathbf{q}_p+\mathbf{q}}, \hat{\mathcal{V}}_{xp}] = \sqrt{n_x}\sum_{k_z} g_{xp}(\mathbf{q}, k_z)(\hat{c}_{\mathbf{q},k_z} - \hat{c}^\dagger_{-\mathbf{q},k_z}). \tag{A18}$$

6. General results about the coupling to a bath

Cavity photons are coupled to a 3D continuum of extracavity photons, while excitons are coupled to a 3D continuum of lattice phonons. The coupling is, respectively, described by Eqs. (7) and (11). In both cases, it corresponds to a linear coupling to a bath of harmonic oscillators, namely a coupling which generically takes the form:

$$\hat{\mathcal{H}}_{\mathrm{bath}}/\hbar = \sum_{\mathbf{q}}\left[\hat{a}^\dagger_{\mathbf{q}}\sum_{k_z}(x_{\mathbf{q},k_z}\hat{\alpha}_{\mathbf{q},k_z} + y_{\mathbf{q},k_z}\hat{\alpha}^\dagger_{-\mathbf{q},k_z}) + \mathrm{H.c.}\right] + \sum_{\mathbf{q},k_z}\omega_{\mathbf{q},k_z}\hat{\alpha}^\dagger_{\mathbf{q},k_z}\hat{\alpha}_{\mathbf{q},k_z}, \tag{A19}$$

with $\hat{a}_{\mathbf{q}}$ either the cavity photon or cavity exciton, and $\hat{\alpha}_{\mathbf{q},k_z}$ either the output photons or the lattice phonons. We now derive the contribution to the EOM of the $\hat{a}_{\mathbf{q}}$ operators resulting from such a generic coupling. We first write the EOM for the bath operators:

$$\partial_t\hat{\alpha}_{\mathbf{q},k_z} = (-i/\hbar)[\hat{\alpha}_{\mathbf{q},k_z}, \hat{\mathcal{H}}_{\mathrm{bath}}] = -i[y_{-\mathbf{q},k_z}\hat{a}^\dagger_{-\mathbf{q}} + x^*_{\mathbf{q},k_z}\hat{a}_{\mathbf{q}} + \omega_{\mathbf{q},k_z}\hat{\alpha}_{\mathbf{q},k_z}]. \tag{A20}$$

The formal solution reads:

$$\alpha_{\mathbf{q},k_z}(t) = e^{-i\omega_{\mathbf{q},k_z}(t-t_0)} - i\int_{t_0}^{t} d\tau e^{-i\omega_{\mathbf{q},k_z}(t-\tau)} \times [x^*_{\mathbf{q},k_z}\hat{a}_{\mathbf{q}}(\tau) + y_{-\mathbf{q},k_z}\hat{a}^\dagger_{-\mathbf{q}}(\tau)]. \tag{A21}$$

On the other hand, the contribution to the EOM for the system operators $\hat{a}_{\mathbf{q}}$ stemming from coupling to the bath reads:

$$(-i/\hbar)[\hat{a}_{\mathbf{q}}(t), \hat{\mathcal{H}}_{\mathrm{bath}}] = -i\sum_{k_z}[x_{\mathbf{q},k_z}\hat{\alpha}_{\mathbf{q},k_z} + y_{\mathbf{q},k_z}\hat{\alpha}^\dagger_{-\mathbf{q},k_z}]. \tag{A22}$$

Injecting the formal solution of Eq. (A21) for the bath operators into Eq. (A21) yields a contribution to the EOM of the form:

$$(-i/\hbar)[\hat{a}_{\mathbf{q}}(t), \hat{\mathcal{H}}_{\mathrm{bath}}] = \hat{F}^{(x)}_{\mathbf{q}}(t) - [\hat{F}^{(y)}_{-\mathbf{q}}(t)]^\dagger - \int_{-\infty}^{\infty} d\tau\{\Gamma_1(t-\tau)\hat{a}_{\mathbf{q}}(\tau) + \Gamma_2(t-\tau)\hat{a}^\dagger_{-\mathbf{q}}(\tau)\}. \tag{A23}$$

We have introduced the so-called Langevin forces:

$$\hat{F}^{(x)}_{\mathbf{q}}(t) = -i\sum_{k_z} x_{\mathbf{q},k_z}\hat{\alpha}_{\mathbf{q},k_z}(t_0)e^{-i\omega_{\mathbf{q},k_z}(t-t_0)} \tag{A24}$$

and

$$\hat{F}^{(y)}_{\mathbf{q}}(t) = -i\sum_{k_z} y_{\mathbf{q},k_z}\hat{\alpha}_{\mathbf{q},k_z}(t_0)e^{-i\omega_{\mathbf{q},k_z}(t-t_0)}. \tag{A25}$$

We have also introduced the damping kernels:

$$\Gamma_1(t) = \Theta(t)\sum_{k_z}(|x_{\mathbf{q},k_z}|^2 e^{-i\omega_{\mathbf{q},k_z}t} + |y_{\mathbf{q},k_z}|^2 e^{i\omega_{-\mathbf{q},k_z}t}) \tag{A26}$$

and

$$\Gamma_2(t) = \Theta(t)\sum_{k_z}(x_{\mathbf{q},k_z}y_{-\mathbf{q},k_z}e^{-i\omega_{\mathbf{q},k_z}t} + x_{-\mathbf{q},k_z}y_{\mathbf{q},k_z}e^{i\omega_{-\mathbf{q},k_z}t}) \tag{A27}$$

(Θ is the Heaviside step function). Note that in the integral over the damping kernels, we have sent the initial time t_0 to $-\infty$, which amounts to assuming that the support of the damping kernel (a few times the memory of the bath) is much smaller than $t - t_0$ (Markov approximation).

The Langevin forces contributions [$\hat{F}$ terms in Eq. (A23)] describe the forcing of the system by the external bath. The integral with the Γ terms in Eq. (A23) (Γ terms) describes the damping induced by the coupling to the bath, giving rise to a finite linewidth to Bogoliubov excitations.

Photonic bath. Specifying these results to our model, we obtain for cavity photons [cf. Eq. (A15): $x_{\mathbf{q},k_z} = \kappa_{\mathbf{q},k_z}$]

$$-\frac{i}{\hbar}[\hat{a}_{\mathbf{q}}(t), \hat{\mathcal{V}}_{\mathrm{out}}] = \hat{F}_{\mathbf{q}}(t) - \int_{-\infty}^{\infty} d\tau\gamma_{c,\mathbf{q}}(t-\tau)\hat{a}_{\mathbf{q}}(\tau), \tag{A28}$$

with the Langevin force

$$\hat{F}_{\mathbf{q}}(t) = -i\sum_{k_z}\kappa_{\mathbf{q},k_z}\hat{\alpha}^{(\mathrm{in})}_{\mathbf{q},k_z}e^{-i\omega^{(\alpha)}_{\mathbf{q},k_z}t}, \tag{A29}$$

with the input modes defined according to $\hat{\alpha}^{(\mathrm{in})}_{\mathbf{q},k_z} := \hat{\alpha}_{\mathbf{q},k_z}(t_0)e^{i\omega^{(\alpha)}_{\mathbf{q},k_z}t_0}$, and with the damping kernel

$$\gamma_{c,\mathbf{q}}(t) = \Theta(t)\sum_{k_z}|\kappa_{\mathbf{q},k_z}|^2 e^{-i\omega^{(\alpha)}_{\mathbf{q},k_z}t}. \tag{A30}$$

Phononic bath. For cavity excitons which are coupled to the bath of thermal lattice solid-state phonons [cf. Eq. (A18): $x_{\mathbf{q},k_z} = i\sqrt{n_x}g_{xp}(\mathbf{q}, k_z) = -y_{\mathbf{q},k_z}$], we find the contribution to EOM:

$$-\frac{i}{\hbar}[\hat{b}_{\mathbf{q}_p+\mathbf{q}}(t),\hat{\mathcal{V}}_{xp}]=\hat{f}_{\mathbf{q}}(t)-[\hat{f}_{-\mathbf{q}}(t)]^\dagger-\int_{-\infty}^{\infty}d\tau[\gamma_{x,\mathbf{q}}(t-\tau)-\gamma^*_{x,-\mathbf{q}}(t-\tau)][\hat{b}_{\mathbf{q}_p+\mathbf{q}}(\tau)+\hat{b}^\dagger_{\mathbf{q}_p-\mathbf{q}}(\tau)], \tag{A31}$$

where we have introduced the Langevin forces,

$$\hat{f}_{\mathbf{q}}(t)=\sqrt{n_x}\sum_{k_z}g_{xp}(\mathbf{q},k_z)\hat{c}^{(\mathrm{in})}_{\mathbf{q},k_z}e^{-i\omega^{(\mathrm{ph})}_{\mathbf{q},k_z}t}, \tag{A32}$$

with the input modes defined according to $\hat{c}^{(\mathrm{in})}_{\mathbf{q},k_z}\coloneqq\hat{c}_{\mathbf{q},k_z}(t_0)e^{i\omega^{(\mathrm{ph})}_{\mathbf{q},k_z}t_0}$, as well as the damping kernels,

$$\gamma_{x,\mathbf{q}}(t)=\Theta(t)\sum_{k_z}n_xg^2_{xp}(\mathbf{q},k_z)e^{-i\omega^{(\mathrm{ph})}_{\mathbf{q},k_z}t}. \tag{A33}$$

7. Complete equations of motion in the frequency domain

We shall gather all terms of the EOM and write them in the frequency domain.

Conventions for Fourier transforms. We first recall the notations for the Fourier transform of the operators:

$$\hat{O}(\omega)=\int_{-\infty}^{\infty}dte^{i\omega t}\hat{O}(t), \tag{A34}$$

$$\hat{O}(t)=\frac{1}{2\pi}\int_{-\infty}^{\infty}d\omega e^{-i\omega t}\hat{O}(\omega). \tag{A35}$$

Note that this convention implies the relation:

$$\hat{O}^\dagger(\omega)=[\hat{O}(-\omega)]^\dagger. \tag{A36}$$

Photon Langevin forces. The photon Langevin force Eq. (A29) reads in Fourier space:

$$\hat{F}_{\mathbf{q}}(\omega)=-i\sum_{k_z}\kappa_{\mathbf{q},k_z}\hat{\alpha}^{(\mathrm{in})}_{\mathbf{q},k_z}\int_{-\infty}^{\infty}dte^{i(\omega-\omega^{(\alpha)}_{\mathbf{q},k_z})t}$$
$$=-i\sum_{k_z}\kappa_{\mathbf{q},k_z}\hat{\alpha}^{(\mathrm{in})}_{\mathbf{q},k_z}2\pi\delta(\omega-\omega^{(\alpha)}_{\mathbf{q},k_z}). \tag{A37}$$

Introducing the partial density of states $\rho_{\mathbf{q},\omega}=\sum_{k_z}\delta(\omega-\omega^{(\alpha)}_{\mathbf{q},k_z})$, we rewrite the photon Langevin force as

$$\hat{F}_{\mathbf{q}}(\omega)=-i\kappa_{\mathbf{q},k_z(\omega)}2\pi\rho_{\mathbf{q},\omega}\hat{\alpha}^{(\mathrm{in})}_{\mathbf{q},k_z(\omega)}, \tag{A38}$$

where $k_z(\omega)$ is such that $\omega^{(\alpha)}_{\mathbf{q},k_z}=\omega$. It will be convenient to replace the label $k_z(\omega)$ by simply ω.

Phonon Langevin forces. The Langevin forces for the phonons, Eq. (A32), have a similar expression:

$$\hat{f}_{\mathbf{q}}(\omega)=\sqrt{n_x}g_{xp}(\mathbf{q},\omega)2\pi\rho'_{\mathbf{q},\omega}\hat{c}^{(\mathrm{in})}_{\mathbf{q},\omega}, \tag{A39}$$

where the phonon partial density of states is $\rho'_{\mathbf{q},\omega}=\sum_{k_z}\delta(\omega-\omega^{(\mathrm{ph})}_{\mathbf{q},k_z})$, and we defined $\hat{c}^{(\mathrm{in})}_{\mathbf{q},\omega}\coloneqq\hat{c}^{(\mathrm{in})}_{\mathbf{q},k'_z}$, where k'_z is such that $\omega=\omega'_{\mathbf{q},k'_z}$. We defined similarly $g_{xp}(\mathbf{q},\omega)\coloneqq g_{xp}(\mathbf{q},k'_z)$. Importantly, the density of states vanishes for $\omega<0$, and therefore $\hat{f}^\dagger_{\mathbf{q}}(\omega)=[\hat{f}_{\mathbf{q}}(-\omega)]^\dagger$ vanishes for $\omega>0$.

Polariton EOM in the frequency domain. We are now ready to write down the complete EOM for the polaritons in the frequency domain. Gathering all contributions to the cavity photons' and excitons' EOM, we find

$$-i\omega\hat{a}_{\mathbf{q}_p+\mathbf{q}}(\omega)=-i\omega^{(0)}_{c,\mathbf{q}_p+\mathbf{q}}\hat{a}_{\mathbf{q}_p+\mathbf{q}}(\omega)-i\frac{\Omega}{2}\hat{b}_{\mathbf{q}_p+\mathbf{q}}(\omega)+i(g_sn_x/2)[\hat{b}^\dagger_{\mathbf{q}_p-\mathbf{q}}(\omega)+2\hat{b}_{\mathbf{q}_p+\mathbf{q}}(\omega)]$$
$$+\hat{F}_{\mathbf{q}_p+\mathbf{q}}(\omega)-\gamma_{c,\mathbf{q}_p+\mathbf{q}}(\omega)\hat{a}_{\mathbf{q}_p+\mathbf{q}}(\omega) \tag{A40}$$

and

$$-i\omega\hat{b}_{\mathbf{q}_p+\mathbf{q}}(\omega)=-i\omega^{(0)}_{x,\mathbf{q}_p+\mathbf{q}}\hat{b}_{\mathbf{q}_p+\mathbf{q}}(\omega)-i\frac{\Omega}{2}\hat{a}_{\mathbf{q}_p+\mathbf{q}}(\omega)+i(g_sn_x/2)[\hat{a}^\dagger_{\mathbf{q}_p-\mathbf{q}}(\omega)+2\hat{a}_{\mathbf{q}_p+\mathbf{q}}(\omega)]$$
$$-ig_xn_x[\hat{b}^\dagger_{\mathbf{q}_p-\mathbf{q}}(\omega)+2\hat{b}_{\mathbf{q}_p+\mathbf{q}}(\omega)]+ig_s\sqrt{n_xn_c}[e^{-i\phi}\hat{b}^\dagger_{\mathbf{q}_p-\mathbf{q}}(\omega)+(2\cos\phi)\hat{b}_{\mathbf{q}_p+\mathbf{q}}(\omega)]$$
$$+\hat{f}_{\mathbf{q}}(\omega)-\hat{f}^\dagger_{-\mathbf{q}}(\omega)-[\gamma_{x,\mathbf{q}}(\omega)-\gamma^*_{x,-\mathbf{q}}(\omega)][\hat{b}_{\mathbf{q}_p+\mathbf{q}}(\omega)+\hat{b}^\dagger_{\mathbf{q}_p-\mathbf{q}}(\omega)]. \tag{A41}$$

Equivalently, we take the Hermitian conjugate of these last two equalities, use that $[\hat{O}(\omega)]^\dagger=\hat{O}^\dagger(-\omega)$, and change (ω,q) into $(-\omega,-q)$. We obtain

$$-i\omega\hat{a}^\dagger_{\mathbf{q}_p-\mathbf{q}}(\omega)=i\omega^{(0)}_{c,\mathbf{q}_p-\mathbf{q}}\hat{a}^\dagger_{\mathbf{q}_p-\mathbf{q}}(\omega)+i\frac{\Omega}{2}\hat{b}^\dagger_{\mathbf{q}_p-\mathbf{q}}(\omega)-i(g_sn_x/2)[\hat{b}_{\mathbf{q}_p+\mathbf{q}}(\omega)+2\hat{b}^\dagger_{\mathbf{q}_p-\mathbf{q}}(\omega)]$$
$$+\hat{F}^\dagger_{\mathbf{q}_p-\mathbf{q}}(\omega)-\gamma^*_{c,\mathbf{q}_p-\mathbf{q}}(\omega)\hat{a}^\dagger_{\mathbf{q}_p-\mathbf{q}}(\omega) \tag{A42}$$

and

$$\begin{aligned}-i\omega\hat{b}^{\dagger}_{\mathbf{q}_p-\mathbf{q}}(\omega) &= i\omega^{(0)}_{X,\mathbf{q}_p-\mathbf{q}}\hat{b}^{\dagger}_{\mathbf{q}_p-\mathbf{q}}(\omega) + i\frac{\Omega}{2}\hat{a}^{\dagger}_{\mathbf{q}_p-\mathbf{q}}(\omega) - i(g_s n_x/2)[\hat{a}_{\mathbf{q}_p+\mathbf{q}}(\omega) + 2\hat{a}^{\dagger}_{\mathbf{q}_p-\mathbf{q}}(\omega)]\\ &\quad + ig_x n_x[\hat{b}_{\mathbf{q}_p+\mathbf{q}}(\omega) + 2\hat{b}^{\dagger}_{\mathbf{q}_p-\mathbf{q}}(\omega)] - ig_s\sqrt{n_x n_c}[e^{i\phi}\hat{b}_{\mathbf{q}_p+\mathbf{q}}(\omega) + (2\cos\phi)\hat{b}^{\dagger}_{\mathbf{q}_p-\mathbf{q}}(\omega)]\\ &\quad + \hat{f}^{\dagger}_{-\mathbf{q}}(\omega) - \hat{f}_{\mathbf{q}}(\omega) - [\gamma^{*}_{x,-\mathbf{q}}(\omega) - \gamma_{x,\mathbf{q}}(\omega)][\hat{b}_{\mathbf{q}_p+\mathbf{q}}(\omega) + \hat{b}^{\dagger}_{\mathbf{q}_p-\mathbf{q}}(\omega)]. \qquad \text{(A43)}\end{aligned}$$

We introduce the notations

$$\tilde{\gamma}_{x,\mathbf{q}}(\omega) = \gamma_{x,\mathbf{q}}(\omega) - \gamma^{*}_{x,-\mathbf{q}}(\omega). \qquad \text{(A44)}$$

$$\gamma_{\text{cav}} = \gamma_{c,\mathbf{q}}(\omega), \qquad \text{(A45)}$$

$$\mu_s = g_s n_x/2, \qquad \text{(A46)}$$

$$\mu_{sx} = g_x n_x - g_s\sqrt{n_x n_c}e^{-i\phi}, \qquad \text{(A47)}$$

where the photonic loss rate γ_{cav} is taken as a real number (namely, we ignore any Lamb shift on the resonance frequencies that would stem from its imaginary part, and that is not observed in the experiment), and approximately frequency and momentum independent. The equations of motion can be finally summarized as

$$\begin{pmatrix}\hat{a}_{\mathbf{q}_p+\mathbf{q}}(\omega)\\ \hat{b}_{\mathbf{q}_p+\mathbf{q}}(\omega)\\ \hat{a}^{\dagger}_{\mathbf{q}_p-\mathbf{q}}(\omega)\\ \hat{b}^{\dagger}_{\mathbf{q}_p-\mathbf{q}}(\omega)\end{pmatrix} = i[\omega\mathbf{1} - \tilde{M}_{\mathbf{q}}]^{-1}\begin{pmatrix}\hat{F}_{\mathbf{q}_p+\mathbf{q}}(\omega)\\ \hat{f}_{\mathbf{q}}(\omega) - \hat{f}^{\dagger}_{-\mathbf{q}}(\omega)\\ \hat{F}^{\dagger}_{\mathbf{q}_p-\mathbf{q}}(\omega)\\ f^{\dagger}_{-\mathbf{q}}(\omega) - \hat{f}_{\mathbf{q}}(\omega)\end{pmatrix}, \qquad \text{(A48)}$$

where we introduced the $\tilde{M}_{\mathbf{q}}$ matrix:

$$\tilde{M}_{\mathbf{q}} = \begin{pmatrix}\omega^{(0)}_{c,\mathbf{q}_p+\mathbf{q}} - i\gamma_{\text{cav}} & \Omega/2 - 2\mu_s & 0 & -\mu_s\\ -2\mu_s + \Omega/2 & \omega^{(0)}_{x,\mathbf{q}_p+\mathbf{q}} + 2\text{Re}(\mu_{sx}) - i\tilde{\gamma}_x & -\mu_s & \mu_{sx} - i\tilde{\gamma}_x\\ 0 & \mu_s & -\omega^{(0)}_{c,\mathbf{q}_p-\mathbf{q}} - i\gamma_{\text{cav}} & -\Omega/2 + 2\mu_s\\ \mu_s & -\mu^{*}_{sx} + i\tilde{\gamma}_x & 2\mu_s - \Omega/2 & -\omega^{(0)}_{x,\mathbf{q}_p-\mathbf{q}} - 2\text{Re}(\mu_{sx}) + i\tilde{\gamma}_x\end{pmatrix}. \qquad \text{(A49)}$$

Phenomenological damping terms. We notice that the exciton damping term $\tilde{\gamma}_x$ as predicted by the phononic bath model does not quantitatively account for the linewidth as measured experimentally. As a matter of fact, the finite linewidth of the excitons $\gamma_x(\mathbf{q})$ is caused by further decoherence mechanisms independent of the coupling to phonons, and we do not attempt to model it directly. Therefore, to faithfully model the experiment we neglect the $\tilde{\gamma}_x$ terms in the $\tilde{M}_{\mathbf{q}}$ matrix of Eq. (A49) and add a phenomenological term $\gamma_x(\mathbf{q})$, such that it results in a complete polaritonic linewidth $\gamma_{\mathbf{q}}$ that agree with the experiment. This leads to the expression of the $M_{\mathbf{q}}$ matrix as given by Eq. (15) of the main text.

Bogoliubov coefficients. As mentioned in the main text, the $M_{\mathbf{q}}$ matrix is brought onto a diagonal form by $P_{\mathbf{q}}M_{\mathbf{q}}P^{-1}_{\mathbf{q}}$, with $P_{\mathbf{q}}$ containing the Bogoliubov coefficients u, v:

$$P_{\mathbf{q}} = \begin{pmatrix}u_{\text{LP},c,\mathbf{q}} & u_{\text{LP},x,\mathbf{q}} & v_{\text{LP},c,-\mathbf{q}} & v_{\text{LP},x,-\mathbf{q}}\\ u_{\text{UP},c,\mathbf{q}} & u_{\text{UP},x,\mathbf{q}} & v_{\text{UP},c,-\mathbf{q}} & v_{\text{UP},x,-\mathbf{q}}\\ v^{*}_{\text{LP},c,\mathbf{q}} & v^{*}_{\text{LP},x,\mathbf{q}} & u^{*}_{\text{LP},c,-\mathbf{q}} & u^{*}_{\text{LP},x,-\mathbf{q}}\\ v^{*}_{\text{UP},c,\mathbf{q}} & v^{*}_{\text{UP},x,\mathbf{q}} & u^{*}_{\text{UP},c,-\mathbf{q}} & u^{*}_{\text{UP},x,-\mathbf{q}}\end{pmatrix}, \qquad \text{(A50)}$$

where the $\mathbf{q_p}$ dependence has been dropped for the sake of lighter notations.

8. Approximate decoupling between the upper and lower polariton

In this section, we derive an approximate model assuming that the lower polariton and upper polariton do not hybridize under Bogoliubov transformation. This allows us to obtain analytical expressions for the frequencies and

Bogoliubov coefficients which are in excellent agreement with the initial model. Using the further approximation that the Bogoliubov coefficients are real, which we shall justify, we show that all four Bogoliubov coefficients for the LP can be reconstructed from the experimentally measured ratio of ghost to normal branch signals. This allows us to reconstruct from the experimental data the quantity $|u_{x,\mathbf{q}} - v_{x,-\mathbf{q}}|^2$, characterizing the decoupling from lattice phonons, and discussed in Sec. IV B. Our starting point is the matrix $M_\mathbf{q}$ [Eq. (15) of the main text] expressed as

$$M_\mathbf{q} = \begin{pmatrix} A_\mathbf{q} & B \\ -B^* & -A_{-\mathbf{q}} \end{pmatrix}, \tag{A51}$$

with

$$A_\mathbf{q} = A_\mathbf{q}^* = A_\mathbf{q}^t = \begin{pmatrix} \omega_{c,\mathbf{q}_p+\mathbf{q}}^{(0)} & \Omega/2 - 2\mu_s \\ \Omega/2 - 2\mu_s & \omega_{x,\mathbf{q}_p+\mathbf{q}}^{(0)} + 2\mathrm{Re}(\mu_{sx}) \end{pmatrix} \tag{A52}$$

and

$$B = B^t = \begin{pmatrix} 0 & -\mu_s \\ -\mu_s & \mu_{sx} \end{pmatrix}. \tag{A53}$$

For the sake of notation, we omit $\mathbf{q}_p$ in the labels; in all expressions, one should make the substitution $\pm\mathbf{q} \to \mathbf{q}_p \pm \mathbf{q}$. We first perform a unitary transformation to the (noninteracting) polariton basis. We introduce the 2×2 unitary matrix U_0 that diagonalizes the noninteracting problem ($\mu_s = \mu_{sx} = 0$); namely,

$$U_{0,\mathbf{q}} = \begin{pmatrix} C_\mathbf{q} & -X_\mathbf{q} \\ X_\mathbf{q} & C_\mathbf{q} \end{pmatrix}, \tag{A54}$$

with

$$U_{0,\mathbf{q}}^t \begin{pmatrix} \omega_{c,\mathbf{q}}^{(0)} & \Omega/2 \\ \Omega/2 & \omega_{x,\mathbf{q}}^{(0)} \end{pmatrix} U_{0,\mathbf{q}} = \begin{pmatrix} \omega_{\mathrm{LP},\mathbf{q}}^{(0)} & 0 \\ 0 & \omega_{\mathrm{UP},\mathbf{q}}^{(0)} \end{pmatrix}, \tag{A55}$$

with the noninteracting resonance frequencies,

$$\omega_{\mathrm{LP/UP},\mathbf{q}}^{(0)} = \frac{\omega_{c,\mathbf{q}}^{(0)} + \omega_{x,\mathbf{q}}^{(0)}}{2} \mp \frac{1}{2}\sqrt{[\omega_{c,\mathbf{q}}^{(0)} - \omega_{x,\mathbf{q}}^{(0)}]^2 + \Omega^2}. \tag{A56}$$

The so-called Hopfield coefficients $X_\mathbf{q}$ and $C_\mathbf{q}$ are real and define the lower and upper polariton operators via

$$\hat{a}_{\mathrm{LP},\mathbf{q}} = C_\mathbf{q}\hat{a}_\mathbf{q} + X_\mathbf{q}\hat{b}_\mathbf{q}, \tag{A57}$$

$$\hat{a}_{\mathrm{UP},\mathbf{q}} = -X_\mathbf{q}\hat{a}_\mathbf{q} + C_\mathbf{q}\hat{b}_\mathbf{q}. \tag{A58}$$

We then write the $M_\mathbf{q}$ matrix in this basis; namely,

$$\begin{aligned} M'_\mathbf{q} &= \begin{pmatrix} U_{0,\mathbf{q}}^t & 0 \\ 0 & U_{0,-\mathbf{q}}^t \end{pmatrix} M_\mathbf{q} \begin{pmatrix} U_{0,\mathbf{q}} & 0 \\ 0 & U_{0,-\mathbf{q}} \end{pmatrix} \\ &= \begin{pmatrix} A'_\mathbf{q} & B'_\mathbf{q} \\ -(B'_{-\mathbf{q}})^* & -A'_{-\mathbf{q}} \end{pmatrix}. \end{aligned} \tag{A59}$$

We have to evaluate the matrices $A'_\mathbf{q} = U_{0,\mathbf{q}}^t A_\mathbf{q} U_{0,\mathbf{q}}$ and $B'_\mathbf{q} = U_{0,\mathbf{q}}^t B U_{0,-\mathbf{q}}$. The final result is

$$A'_\mathbf{q} = \begin{pmatrix} \omega_{\mathrm{LP},\mathbf{q}}^{(0)} + 2\mathrm{Re}(gn)_{\mathrm{LL},\mathbf{q},\mathbf{q}} & 2\mathrm{Re}(gn)_{\mathrm{LU},\mathbf{q},\mathbf{q}} \\ 2\mathrm{Re}(gn)_{\mathrm{LU},\mathbf{q},\mathbf{q}} & \omega_{\mathrm{UP},\mathbf{q}}^{(0)} + 2\mathrm{Re}(gn)_{\mathrm{UU},\mathbf{q},\mathbf{q}} \end{pmatrix}, \tag{A60}$$

$$B'_\mathbf{q} = \begin{pmatrix} (gn)_{\mathrm{LL},\mathbf{q},-\mathbf{q}} & (gn)_{\mathrm{LU},\mathbf{q},-\mathbf{q}} \\ (gn)_{\mathrm{LU},\mathbf{q},-\mathbf{q}} & (gn)_{\mathrm{UU},\mathbf{q},-\mathbf{q}} \end{pmatrix}, \tag{A61}$$

where we define the (q-dependent) effective interactions as

$$\begin{aligned} (gn)_{\mathrm{LL},\mathbf{q},\mathbf{q}'} &= -(C_\mathbf{q}X_{\mathbf{q}'} + X_\mathbf{q}C_{\mathbf{q}'})\mu_s + X_\mathbf{q}X_{\mathbf{q}'}\mu_{sx}, \\ (gn)_{\mathrm{UU},\mathbf{q},\mathbf{q}'} &= (C_\mathbf{q}X_{\mathbf{q}'} + X_\mathbf{q}C_{\mathbf{q}'})\mu_s + C_\mathbf{q}C_{\mathbf{q}'}\mu_{sx}, \\ (gn)_{\mathrm{LU},\mathbf{q},\mathbf{q}'} &= (X_\mathbf{q}X_{\mathbf{q}'} - C_\mathbf{q}C_{\mathbf{q}'})\mu_s + X_\mathbf{q}C_{\mathbf{q}'}\mu_{sx}. \end{aligned}$$

We now make the simplification that the upper and lower polaritons do not hybridize; namely, we set $(gn)_{\mathrm{LU}} = 0$. The $M'_\mathbf{q}$ matrix then splits into two independent 2×2 matrices, describing independent Bogoliubov transformations for the upper and lower polaritons. We have verified that, in the conditions of the experiment, the coefficients of the (2×2) Bogoliubov transformations found in this approximation are almost identical to the exact coefficients obtained from $M'_\mathbf{q}$. We then have two matrices to diagonalize:

$$M'_{\mathrm{LP},\mathbf{q}} = \begin{pmatrix} a_\mathbf{q} & b_\mathbf{q} \\ -b_{-\mathbf{q}}^* & -a_{-\mathbf{q}} \end{pmatrix}, \tag{A62}$$

with

$$a_\mathbf{q} := \omega_{\mathrm{LP},\mathbf{q}}^{(0)} + 2\mathrm{Re}(gn)_{\mathrm{LL},\mathbf{q},\mathbf{q}}, \tag{A63}$$

$$b_{-\mathbf{q}} := (gn)_{\mathrm{LL},\mathbf{q},-\mathbf{q}}, \tag{A64}$$

for the LP, and similarly for the UP with $a_\mathbf{q} = \omega_{\mathrm{UP},\mathbf{q}}^{(0)} + 2\mathrm{Re}(gn)_{\mathrm{UU},\mathbf{q},\mathbf{q}}$ and $b_\mathbf{q} = (gn)_{\mathrm{UU},\mathbf{q},-\mathbf{q}}$. The diagonalization is of the form:

$$M'_{\mathrm{LP},\mathbf{q}} = \begin{pmatrix} u_\mathbf{q}^* & -v_\mathbf{q} \\ -v_{-\mathbf{q}}^* & u_{-\mathbf{q}} \end{pmatrix} \begin{pmatrix} \omega_{\mathrm{LP},\mathbf{q}} & 0 \\ 0 & -\omega_{\mathrm{LP},-\mathbf{q}} \end{pmatrix} \begin{pmatrix} u_\mathbf{q} & v_{-\mathbf{q}} \\ v_\mathbf{q}^* & u_{-\mathbf{q}}^* \end{pmatrix}, \tag{A65}$$

where we introduce the u and v Bogoliubov coefficients associated to the lower polariton. As we shall only be

interested in the lower polariton u, v coefficients, we omit their LP labels. $\omega_{\mathrm{LP},\mathbf{q}}$ gives the LP dispersion relation in the presence of interactions. Similarly, for the UP the eigenvalues of $M'_{\mathrm{UP},\mathbf{q}}$, namely $\omega_{\mathrm{UP},\mathbf{q}}$ and $-\omega_{\mathrm{UP},-\mathbf{q}}$, give the UP dispersion relation in the presence of interactions. Given that $\mathrm{Re}(gn)_{\mathrm{UU}} \ll \omega^{(0)}_{\mathrm{UP},\mathbf{q}}$ for all relevant $\mathbf{q}$'s, the matrix $M'_{\mathrm{UP},\mathbf{q}}$ is almost diagonal, and therefore the Bogoliubov eigenmodes are almost identical to the noninteracting upper polaritons (the Bogoliubov transformation diagonalizing $M'_{\mathrm{UP},\mathbf{q}}$ is close to the identity, something which we verified numerically).

We now explicitly proceed to the diagonalization of the $M'_{\mathrm{LP},\mathbf{q}}$ matrix in Eq. (A62). Note that $b_{-\mathbf{q}} = b_{\mathbf{q}}$. We then write:

$$M'_{\mathrm{LP},\mathbf{q}} = \frac{a_{\mathbf{q}} - a_{-\mathbf{q}}}{2}\mathbf{1} + \begin{pmatrix} \bar{a}_{\mathbf{q}} & b_{\mathbf{q}} \\ -b^*_{\mathbf{q}} & -\bar{a}_{\mathbf{q}} \end{pmatrix}, \tag{A66}$$

with $\bar{a}_{\mathbf{q}} = (a_{\mathbf{q}} + a_{-\mathbf{q}})/2$. The eigenvalues of $M'_{\mathrm{LP},\mathbf{q}}$ are then $\omega_{\mathrm{LP},\mathbf{q}}$ and $-\omega_{\mathrm{LP},-\mathbf{q}}$, with

$$\omega_{\mathrm{LP},\mathbf{q}} = \frac{a_{\mathbf{q}} - a_{-\mathbf{q}}}{2} + \sqrt{\bar{a}^2_{\mathbf{q}} - |b_{\mathbf{q}}|^2}. \tag{A67}$$

We introduce the notation $\tilde{\omega}_{\mathbf{q}} = \sqrt{\bar{a}^2_{\mathbf{q}} - |b_{\mathbf{q}}|^2}$. Note that we focus on the regime where $\bar{a}^2_{\mathbf{q}} > |b_{\mathbf{q}}|^2$, which is always the case in the regime accessible to our measurements. Otherwise, the eigenvalues have an imaginary part, and we find that $|u_{\mathbf{q}}|^2 = |v_{\mathbf{q}}|^2$, so that the eigenmodes do not describe proper bosonic excitations. This latter case corresponds to the flat part in the excitation spectrum, which shall not be discussed further in this paper. Solving the eigenvalue equations using the conventions of Eq. (A65), the convention that $u_{\mathbf{q}}$ is real, and the normalization condition $|u_{\mathbf{q}}|^2 - |v_{\mathbf{q}}|^2 = 1$, we find the coefficients

$$u_{\mathbf{q}} = u_{-\mathbf{q}} = \sqrt{\frac{\bar{a}_{\mathbf{q}}}{2\tilde{\omega}_{\mathbf{q}}} + \frac{1}{2}}, \tag{A68}$$

$$v_{\mathbf{q}} = v_{-\mathbf{q}} = \frac{b_{\mathbf{q}}}{|b_{\mathbf{q}}|}\sqrt{\frac{\bar{a}_{\mathbf{q}}}{2\tilde{\omega}_{\mathbf{q}}} - \frac{1}{2}}. \tag{A69}$$

Note in particular that the $v_{\mathbf{q}}$ coefficient is complex, with a phase given by the phase of $b_{\mathbf{q}} = (gn)_{\mathrm{LL},\mathbf{q},-\mathbf{q}}$. In practice, though, this phase is negligible, and we take $v_{\mathbf{q}}$ real.

The Bogoliubov eigenmode of the lower polariton is described by the annihilation operator (recall that a nonzero pump momentum $\mathbf{q}_p$ should be reintroduced in these expressions: $\pm\mathbf{q} \to \mathbf{q}_p \pm \mathbf{q}$):

$$\hat{\beta}_{\mathrm{LP},\mathbf{q}} = u_{\mathbf{q}}\hat{a}_{\mathrm{LP},\mathbf{q}} + v_{-\mathbf{q}}\hat{a}^\dagger_{\mathrm{LP},-\mathbf{q}} \tag{A70}$$

$$= u_{\mathbf{q}}(C_{\mathbf{q}}\hat{a}_{\mathbf{q}} + X_{\mathbf{q}}\hat{b}_{\mathbf{q}}) + v_{-\mathbf{q}}(C_{-\mathbf{q}}\hat{a}^\dagger_{-\mathbf{q}} + X_{-\mathbf{q}}\hat{b}^\dagger_{-\mathbf{q}}). \tag{A71}$$

We therefore have the identification:

$$u_{\mathrm{LP},c,\mathbf{q}} = u_{\mathbf{q}}C_{\mathbf{q}}, \qquad u_{\mathrm{LP},x,\mathbf{q}} = u_{\mathbf{q}}X_{\mathbf{q}},$$
$$v_{\mathrm{LP},c,-\mathbf{q}} = v_{-\mathbf{q}}C_{-\mathbf{q}}, \qquad v_{\mathrm{LP},x,-\mathbf{q}} = v_{-\mathbf{q}}X_{-\mathbf{q}}. \tag{A72}$$

Therefore, the experimental measurement of $v_{\mathrm{LP},c,-q}/u_{\mathrm{LP},c,q}$ gives direct access to the ratio $v_{-\mathbf{q}}/u_{\mathbf{q}}$ of the lower polariton Bogoliubov transformation. Assuming that $v_{\mathbf{q}} = v_{-\mathbf{q}}$ is real (an excellent approximation in the regime of the experiment), and using the normalization $u^2_{\mathbf{q}} - v^2_{\mathbf{q}} = 1$ valid in the nonflat part of the dispersion relation, we then reconstruct both $u_{\mathbf{q}}$ and $v_{\mathbf{q}}$. Using the knowledge of the Hopfield coefficients $X_{\mathbf{q}}, C_{\mathbf{q}}$ of the noninteracting problem, we may then reconstruct all four Bogoliubov coefficients $u_{c,\mathbf{q}}, u_{x,\mathbf{q}}, v_{c,\mathbf{q}}, v_{x,\mathbf{q}}$, and in particular the thermal decoupling coefficient $|u_{x,\mathbf{q}} - v_{x,-\mathbf{q}}|^2$, which is discussed in Sec. IV B. The quantitative agreement further confirms both the validity of the model as well as the approximate decoupling between LP and UP as discussed in this section.

9. Estimating the exciton-phonon interaction $n_x\gamma_{xp}(\omega)$

In this section, we provide further details and quantitative estimates for the exciton-phonon interaction strength $\gamma_{xp}(\omega)$ introduced in Eq. (23) of the main text. In the limit of strong confinement of excitons in the z direction of the quantum well, the exciton-phonon coupling amplitude is given by

$$\hbar g_{xp}(\mathbf{q}, k_z) = \sqrt{\frac{\hbar\sqrt{\mathbf{q}^2 + k_z^2}}{2\rho V v_s}}(V_e I^p_e I^z_e - V_h I^p_h I^z_h), \tag{A73}$$

where $\rho = 5.3 \times 10^3\ \mathrm{kg\,m^{-3}}$ is GaAs density, $v_s = 4.7 \times 10^3\ \mathrm{ms^{-1}}$ is the longitudinal acoustic speed of sound in GaAs, V is a quantization volume, $V_{e,h} = (-7, 2.7)$ eV are the deformation potentials in GaAs for band-edge electrons and holes, respectively.

$$I^z_e \simeq I^z_h \simeq \exp(-k_z^2/q^2_{z,\mathrm{cut}}) \tag{A74}$$

is a Gaussian approximation of the k_z component of the electron and hole envelope wave function which is assumed to be mostly determined by the quantum well thickness L_z, imposing the cutoff wave vector $q_{z,\mathrm{cut}} \approx 0.9 \times 2\pi/L_z$.

$$I^p_{e(h)} = [1 + (m_{e(h)}/(2M)qa_B)^2]^{-3/2} \tag{A75}$$

is the in-plane component of the electron-hole wave function resulting from its bound state character of Bohr radius $a_B \simeq 10$ nm. $m_{e,h}$ are the electron and hole effective masses and $M = m_e + m_h$ is the excitonic mass. Note that $g_{xp}(\mathbf{q}, k_z) = g_{xp}(\mathbf{q}, -k_z)$, which allows us to replace unambiguously k_z by ω using the dispersion relation $\omega = v_s\sqrt{\mathbf{q}^2 + k_z^2}$. In the parameter regime of the experiment, $q \ll k_z$, so that $\omega \approx v_s|k_z|$. Furthermore, $[m_{e(h)}/$

$(2M)qa_B]^2 \ll 1$. Therefore, the coupling simplifies to

$$\hbar g_{xp}(\omega) = \sqrt{\frac{\hbar\omega}{2\rho V v_s^2}}(V_e - V_h)\exp\left(-\frac{\omega^2}{v_s^2 q_{z,\mathrm{cut}}^2}\right). \quad \text{(A76)}$$

An explicit expression for $\gamma_{xp}(\omega)$ in Eq. (23) can now be determined. We define the excitonic density in the quantum well as $n_x = N_x/A$, where A is the condensate area and $V = AL_z$. The density of states $\rho'_{\mathbf{q},\omega}$ counts the number of phonons' wave vectors k_z matching the condition $\omega = \omega^{(\mathrm{ph})}_{\mathbf{q},k_z} = v_s\sqrt{\mathbf{q}^2 + k_z^2}$; namely, it is such that

$$\rho'_{\mathbf{q},\omega} d\omega = (L_z/2\pi)dk_z. \quad \text{(A77)}$$

Using the fact that in our experiment $v_s|\mathbf{q}| \ll \omega$, we get

$$\rho'_{\mathbf{q},\omega} \approx \Theta(\omega)\frac{L_z}{2\pi v_s}, \quad \text{(A78)}$$

which is approximately constant (Θ is the Heaviside step function). We have further verified numerically the validity of this approximation. So finally,

$$\gamma_{xp}(\omega)n_x = \frac{n_x L_z A}{2v_s}\Theta(\omega)g_{xp}(\omega)^2, \quad \text{(A79)}$$

that can be more explicitly given as

$$\gamma_{xp}(\omega)n_x = \frac{\omega n_x}{4v_s^3\rho\hbar}(V_e - V_h)^2\exp\left(-\frac{2\omega^2}{v_s^2 q_{z,\mathrm{cut}}^2}\right). \quad \text{(A80)}$$

In this expression, the argument in the exponential provides a cutoff wave vector above which the exciton-phonons coupling vanishes. This cutoff can be compared with the experimental one when fitting $A_{\mathrm{LP}}(\theta)[T]$, the measured spectrally-integrated LP emission intensity at phonons temperature T, and in the noninteracting case, with its theoretical expression. The latter is given by Eq. (26) assuming the noninteracting limit for the involved Bogoliubov coefficients. As this measurement is carried out with a very low laser intensity, the phonons temperature matches the sample mount temperature which is measured independently. As a result, the only remaining free parameter fixing the shape of $A_{\mathrm{LP}}(\theta)$ for every temperatures is $q_{z,\mathrm{cut}}$. This analysis yields $L_z = 8.5$ nm instead of the nominal quantum well thickness $L_z = 17$ nm. A good reason for this mismatch is that the strong confinement assumption $a_B > L_z$, with $a_b = 10$ nm, is in fact not well checked in our thick quantum well. In the weaker confinement regime where $a_B < L_z$, the contribution of the bound electron-hole wave function contributes as the shortest length scale and hence contributes more to $q_{z,\mathrm{cut}}^2$ than L_z. The apparent L_z in the strong confinement description is thus expected to decrease by a factor of the order of $\sim L_z/a_B$. Another contribution to this reduced L_z is that the expression $q_{z,\mathrm{cut}} \sim 0.9 \times 2\pi/L_z$ is obtained by fitting the exact wave function in a finite height quantum well with a vertical transition edge between the barriers and the quantum well, while in reality the transition edges are typically much smoother than that due to indium diffusion that can result in tighter confinement length along z for the ground state (see, e.g., Ref. [68]).

APPENDIX B: MAIN EXPERIMENTAL PARAMETERS AND PHYSICAL QUANTITIES

Table I provides a quantitative summary of the physical parameters entering the modeling of our experiment and of the key physical quantities introduced in the article.

TABLE I. Main system parameters and physical quantities.

Notation	Description	Value
$\hbar\omega_{\mathrm{cav}}(\mathbf{q}=0)$	Cavity mode energy	1450.54 meV
$\hbar\omega_x$	Excitonic transition energy	1450.36 meV
$\hbar\omega_{\mathrm{LP}}(\mathbf{q}=0)$	Lower polariton ground state energy	1448.81 meV
$\hbar\omega_{\mathrm{las}}$	Laser to polariton mode detuning	$\hbar\omega_{\mathrm{LP}}(\mathbf{q}=0) + 0.19$ meV
$\hbar\Omega$	Rabi splitting	3.28 meV
$\hbar\gamma_{x,0}$	Excitonic transition linewidth	$\simeq$0.12 meV
β	Momentum dependence parameter of excitonic linewidth	$\simeq$0.045 meVμm^2
$\hbar\gamma_{\mathrm{cav}}$	Cavity mode linewidth	$\simeq$0.025 meV
$\hbar\gamma_{xp}^M$	Max value (over $\mathbf{q}$) of the exciton-phonon interaction strength	$\simeq 5\times10^{-3}$ meVμm^2
n_x	Excitonic density	$[0.32, 3.2]\times10^{11}$ cm^{-2}
$\hbar g_s n_x$	Interaction energy: saturation contribution	0.19 meV
$\hbar g_x n_x$	Interaction energy: Coulomb contribution	$0(-0;+0.3)$ meV
T_c	Temperature: cryostat	[6, 11] K
T	Temperature: thermal phonons bath	[6, 15] K
T_{GN}	For $T \gg T_{GN}$, the normal-ghost brightness ratio is T independent	$\simeq$15 K
T_{EB}	Characteristic temperature: equal normal and ghost mode brightness	$\simeq$5.2 K
$T_{N,G}^{(\mathrm{cr})}(\mathbf{q})$	Crossover temperature: phonon bath to photon vacuum dominated emission	$\gtrsim$1 K

[1] M. Tinkham, *Introduction to Superconductivity*, Dover Books on Physics Series (Dover Publications, New York, 2004).
[2] P. Kapitza, *Viscosity of liquid Helium below the λ-point*, Nature (London) **141**, 74 (1938).
[3] J. F. Allen and A. D. Misener, *Flow of liquid Helium II*, Nature (London) **141**, 75 (1938).
[4] N. Bogoliubov, *On the theory of superfluidity*, J. Phys. **11**, 23 (1947).
[5] L. P. Pitaevskii and S. Stringari, *Bose-Einstein Condensation* (Clarendon Press, Oxford, 2003).
[6] A. P. Chikkatur, A. Görlitz, D. M. Stamper-Kurn, S. Inouye, S. Gupta, and W. Ketterle, *Suppression and enhancement of impurity scattering in a Bose-Einstein condensate*, Phys. Rev. Lett. **85**, 483 (2000).
[7] J. Steinhauer, R. Ozeri, N. Katz, and N. Davidson, *Excitation spectrum of a Bose-Einstein condensate*, Phys. Rev. Lett. **88**, 120407 (2002).
[8] J. M. Vogels, K. Xu, C. Raman, J. R. Abo-Shaeer, and W. Ketterle, *Experimental observation of the Bogoliubov transformation for a Bose-Einstein condensed gas*, Phys. Rev. Lett. **88**, 060402 (2002).
[9] A. Polkovnikov, E. Altman, and E. Demler, *Interference between independent fluctuating condensates*, Proc. Natl. Acad. Sci. U.S.A. **103**, 6125 (2006).
[10] M. Gring, M. Kuhnert, T. Langen, T. Kitagawa, B. Rauer, M. Schreitl, I. Mazets, D. A. Smith, E. Demler, and J. Schmiedmayer, *Relaxation and prethermalization in an isolated quantum system*, Science **337**, 1318 (2012).
[11] T. Langen, R. Geiger, M. Kuhnert, B. Rauer, and J. Schmiedmayer, *Local emergence of thermal correlations in an isolated quantum many-body system*, Nat. Phys. **9**, 640 (2013).
[12] B. Rauer, S. Erne, T. Schwiegler, F. Cataldini, M. Tajik, and J. Schmiedmayer, *Recurrences in an isolated quantum many-body system*, Science **360**, 307 (2018).
[13] P. Christodoulou, M. Gaĺka, N. Dogra, R. Lopes, J. Schmitt, and Z. Hadzibabic, *Observation of first and second sound in a BKT superfluid*, Nature (London) **594**, 191 (2021).
[14] I. Carusotto and C. Ciuti, *Quantum fluids of light*, Rev. Mod. Phys. **85**, 299 (2013).
[15] I. Carusotto and C. Ciuti, *Probing microcavity polariton superfluidity through resonant rayleigh scattering*, Phys. Rev. Lett. **93**, 166401 (2004).
[16] A. Amo, J. Lefrère, S. Pigeon, C. Adrados, C. Ciuti, I. Carusotto, R. Houdré, E. Giacobino, and A. Bramati, *Superfluidity of polaritons in semiconductor microcavities*, Nat. Phys. **5**, 805 (2009).
[17] Q. Fontaine, T. Bienaimé, S. Pigeon, E. Giacobino, A. Bramati, and Q. Glorieux, *Observation of the Bogoliubov dispersion in a fluid of light*, Phys. Rev. Lett. **121**, 183604 (2018).
[18] C. Michel, O. Boughdad, M. Albert, P.-E. Larré, and M. Bellec, *Superfluid motion and drag-force cancellation in a fluid of light*, Nat. Commun. **9**, 2108 (2018).
[19] R. Y. Chiao and J. Boyce, *Bogoliubov dispersion relation and the possibility of superfluidity for weakly interacting photons in a two-dimensional photon fluid*, Phys. Rev. A **60**, 4114 (1999).
[20] V. Kohnle, Y. Léger, M. Wouters, M. Richard, M. T. Portella-Oberli, and B. Deveaud-Plédran, *From single particle to superfluid excitations in a dissipative polariton gas*, Phys. Rev. Lett. **106**, 255302 (2011).
[21] F. Claude, M. J. Jacquet, R. Usciati, I. Carusotto, E. Giacobino, A. Bramati, and Q. Glorieux, *High-resolution coherent probe spectroscopy of a polariton quantum fluid*, Phys. Rev. Lett. **129**, 103601 (2022).
[22] X. Busch, I. Carusotto, and R. Parentani, *Spectrum and entanglement of phonons in quantum fluids of light*, Phys. Rev. A **89**, 043819 (2014).
[23] S. Koghee and M. Wouters, *Dynamical Casimir emission from polariton condensates*, Phys. Rev. Lett. **112**, 036406 (2014).
[24] D. Gerace and I. Carusotto, *Analog Hawking radiation from an acoustic black hole in a flowing polariton superfluid*, Phys. Rev. B **86**, 144505 (2012).
[25] H. S. Nguyen, D. Gerace, I. Carusotto, D. Sanvitto, E. Galopin, A. Lemaître, I. Sagnes, J. Bloch, and A. Amo, *Acoustic black hole in a stationary hydrodynamic flow of microcavity polaritons*, Phys. Rev. Lett. **114**, 036402 (2015).
[26] J. Steinhauer, *Observation of quantum hawking radiation and its entanglement in an analogue black hole*, Nat. Phys. **12**, 959 (2016).
[27] M. J. Jacquet, T. Boulier, F. Claude, A. Maître, E. Cancellieri, C. Adrados, A. Amo, S. Pigeon, Q. Glorieux, A. Bramati, and E. Giacobino, *Polariton fluids for analogue gravity physics*, Phil. Trans. R. Soc. A **378**, 20190225 (2020).
[28] M. J. Jacquet and F. König, *Analytical description of quantum emission in optical analogs to gravity*, Phys. Rev. A **102**, 013725 (2020).
[29] D. Sarchi and I. Carusotto, *Near-field intensity correlations in parametric photoluminescence from a planar microcavity*, Phys. Rev. B **81**, 075320 (2010).
[30] M. V. Regemortel, S. Ravets, A. Imamoglu, I. Carusotto, and M. Wouters, *Engineering Gaussian states of light from a planar microcavity*, SciPost Phys. **5**, 013 (2018).
[31] E. L. Bolda, R. Y. Chiao, and W. H. Zurek, *Dissipative optical flow in a nonlinear Fabry-Pérot cavity*, Phys. Rev. Lett. **86**, 416 (2001).
[32] C. Weisbuch, M. Nishioka, A. Ishikawa, and Y. Arakawa, *Observation of the coupled exciton-photon mode splitting in a semiconductor quantum microcavity*, Phys. Rev. Lett. **69**, 3314 (1992).
[33] B. Deveaud, *The Physics of Semiconductor Microcavities* (Wiley-VCH, Weinheim, 2007).
[34] A. V. Kavokin, J. J. Baumberg, G. Malpuech, and F. P. Laussy, *Microcavities* (Oxford University Press, Oxford, 2017).
[35] J. J. Hopfield, *Theory of the contribution of excitons to the complex dielectric constant of crystals*, Phys. Rev. **112**, 1555 (1958).
[36] C. Ciuti, V. Savona, C. Piermarocchi, A. Quattropani, and P. Schwendimann, *Role of the exchange of carriers in elastic exciton-exciton scattering in quantum wells*, Phys. Rev. B **58**, 7926 (1998).
[37] G. Rochat, C. Ciuti, V. Savona, C. Piermarocchi, A. Quattropani, and P. Schwendimann, *Excitonic Bloch*

equations for a two-dimensional system of interacting excitons, Phys. Rev. B **61**, 13856 (2000).

[38] B. Krummheuer, V. M. Axt, and T. Kuhn, *Theory of pure dephasing and the resulting absorption line shape in semiconductor quantum dots*, Phys. Rev. B **65**, 195313 (2002).

[39] C. Piermarocchi, F. Tassone, V. Savona, A. Quattropani, and P. Schwendimann, *Nonequilibrium dynamics of free quantum-well excitons in time-resolved photoluminescence*, Phys. Rev. B **53**, 15834 (1996).

[40] I. G. Savenko, T. C. H. Liew, and I. A. Shelykh, *Stochastic Gross-Pitaevskii equation for the dynamical thermalization of Bose-Einstein condensates*, Phys. Rev. Lett. **110**, 127402 (2013).

[41] S. Klembt, P. Stepanov, T. Klein, A. Minguzzi, and M. Richard, *Thermal decoherence of a nonequilibrium polariton fluid*, Phys. Rev. Lett. **120**, 035301 (2018).

[42] G. Munoz-Matutano, A. Wood, M. Johnsson, X. Vidal, B. Q. Baragiola, A. Reinhard, A. Lemaître, J. Bloch, A. Amo, G. Nogues, B. Besga, M. Richard, and T. Volz, *Emergence of quantum correlations from interacting fibre-cavity polaritons*, Nat. Mater. **18**, 213 (2019).

[43] L. Scarpelli, C. Elouard, M. Johnsson, M. Morassi, A. Lemaitre, I. Carusotto, J. Bloch, S. Ravets, M. Richard, and T. Volz, *Probing many-body correlations using quantum-cascade correlation spectroscopy*, arXiv:2212.09047.

[44] C. Ciuti and I. Carusotto, *Quantum fluid effects and parametric instabilities in microcavities*, Phys. Status Solidi B **242**, 2224 (2005).

[45] E. Ivchenko, A. Nesvizhskii, and S. Jorda, *Resonant Bragg reflection from quantum-well structures*, Superlattices Microstruct. **16**, 17 (1994).

[46] V. Savona, C. Piermarocchi, A. Quattropani, P. Schwendimann, and F. Tassone, *Optical properties of microcavity polaritons*, Phase Transitions **68**, 169 (1999).

[47] O. Bleu, G. Li, J. Levinsen, and M. M. Parish, *Polariton interactions in microcavities with atomically thin semiconductor layers*, Phys. Rev. Res. **2**, 043185 (2020).

[48] P. M. Walker, L. Tinkler, B. Royall, D. V. Skryabin, I. Farrer, D. A. Ritchie, M. S. Skolnick, and D. N. Krizhanovskii, *Dark solitons in high velocity waveguide polariton fluids*, Phys. Rev. Lett. **119**, 097403 (2017).

[49] P. Stepanov, I. Amelio, J. G. Rousset, J. Bloch, A. Lemaître, A. Amo, A. Minguzzi, I. Carusotto, and M. Richard, *Dispersion relation of the collective excitations in a resonantly driven polariton fluid*, Nat. Commun. **10**, 3869 (2019).

[50] V. Savona, *Effect of interface disorder on quantum well excitons and microcavity polaritons*, J. Phys. Condens. Matter **19**, 295208 (2007).

[51] A. Baas, J. P. Karr, H. Eleuch, and E. Giacobino, *Optical bistability in semiconductor microcavities*, Phys. Rev. A **69**, 023809 (2004).

[52] See Supplemental Material at http://link.aps.org/supplemental/10.1103/PhysRevX.13.041058 for additional experimental measurements, and for details on the data analysis method.

[53] J. M. Zajac and W. Langbein, *Parametric scattering of microcavity polaritons into ghost branches*, Phys. Rev. B **92**, 165305 (2015).

[54] Q. Fontaine, D. Squizzato, F. Baboux, I. Amelio, A. Lemaître, M. Morassi, I. Sagnes, L. L. Gratiet, A. Harouri, M. Wouters, I. Carusotto, A. Amo, M. Richard, A. Minguzzi, L. Canet, S. Ravets, and J. Bloch, *Kardar-Parisi-Zhang universality in a one-dimensional polariton condensate*, Nature (London) **608**, 687 (2022).

[55] M. Wouters and I. Carusotto, *Excitations in a nonequilibrium Bose-Einstein condensate of exciton polaritons*, Phys. Rev. Lett. **99**, 140402 (2007).

[56] D. Ballarini, D. Caputo, G. Dagvadorj, R. Juggins, M. D. Giorgi, L. Dominici, K. West, L. N. Pfeiffer, G. Gigli, M. H. Szymanska, and D. Sanvitto, *Directional Goldstone waves in polariton condensates close to equilibrium*, Nat. Commun. **11**, 217 (2020).

[57] M. Pieczarka, E. Estrecho, M. Boozarjmehr, O. Bleu, M. Steger, K. West, L. N. Pfeiffer, D. W. Snoke, J. Levinsen, M. M. Parish, A. G. Truscott, and E. A. Ostrovskaya, *Observation of quantum depletion in a non-equilibrium exciton-polariton condensate*, Nat. Commun. **11**, 429 (2020).

[58] M. Pieczarka, O. Bleu, E. Estrecho, M. Wurdack, M. Steger, D. W. Snoke, K. West, L. N. Pfeiffer, A. G. Truscott, E. A. Ostrovskaya, J. Levinsen, and M. M. Parish, *Bogoliubov excitations of a polariton condensate in dynamical equilibrium with an incoherent reservoir*, Phys. Rev. B **105**, 224515 (2022).

[59] M. Steger, R. Hanai, A. O. Edelman, P. B. Littlewood, D. W. Snoke, J. Beaumariage, B. Fluegel, K. West, L. N. Pfeiffer, and A. Mascarenhas, *Direct observation of the quantum fluctuation driven amplitude mode in a microcavity polariton condensate*, Phys. Rev. B **103**, 205125 (2021).

[60] I. Amelio, A. Minguzzi, M. Richard, and I. Carusotto, *Galilean boosts and superfluidity of resonantly driven polariton fluids in the presence of an incoherent reservoir*, Phys. Rev. Res. **2**, 023158 (2020).

[61] W. G. Unruh, *Experimental black-hole evaporation?*, Phys. Rev. Lett. **46**, 1351 (1981).

[62] Z. Z. Yan, Y. Ni, C. Robens, and M. W. Zwierlein, *Bose polarons near quantum criticality*, Science **368**, 190 (2020).

[63] M. G. Skou, T. G. Skov, N. B. Jørgensen, K. K. Nielsen, A. Camacho-Guardian, T. Pohl, G. M. Bruun, and J. J. Arlt, *Non-equilibrium quantum dynamics and formation of the Bose polaron*, Nat. Phys. **17**, 731 (2021).

[64] C. J. Myatt, E. A. Burt, R. W. Ghrist, E. A. Cornell, and C. E. Wieman, *Production of two overlapping Bose-Einstein condensates by sympathetic cooling*, Phys. Rev. Lett. **78**, 586 (1997).

[65] E. Timmermans and R. Côté, *Superfluidity in sympathetic cooling with atomic Bose-Einstein condensates*, Phys. Rev. Lett. **80**, 3419 (1998).

[66] M. K. Tey, S. Stellmer, R. Grimm, and F. Schreck, *Double-degenerate Bose-Fermi mixture of strontium*, Phys. Rev. A **82**, 011608(R) (2010).

[67] X.-Y. Chen, M. Duda, A. Schindewolf, R. Bause, I. Bloch, and X.-Y. Luo, *Suppression of unitary three-body loss in a degenerate Bose-Fermi mixture*, Phys. Rev. Lett. **128**, 153401 (2022).

[68] K. Muraki, S. Fukatsu, Y. Shiraki, and R. Ito, *Surface segregation of in atoms and its influence on the quantized levels in* InGaAs/GaAs *quantum wells*, J. Cryst. Growth **127**, 546 (1993).